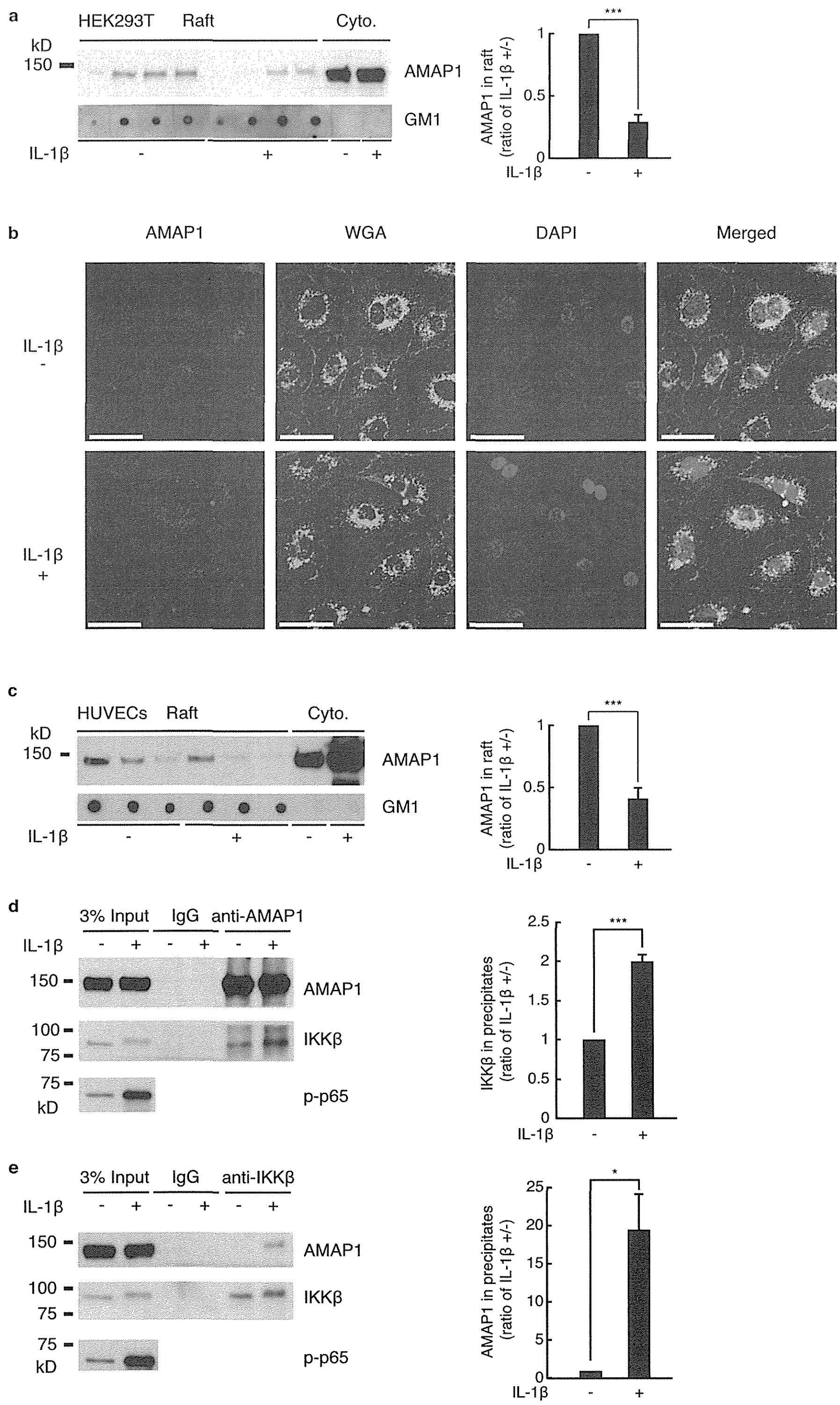

Figure 3 | IL-1β induces AMAP1 translocation and the AMAP1 and IKKβ interaction. (a) Representative AMAP1 immunoblots of fractions from sucrose gradient centrifugation of HEK293T cells treated with or without IL-1β (2.5 ng/mL) for 30 min and the cumulative, quantitative densitometry data from three independent experiments are shown. (b) HUVECs were treated with or without IL-1β (2.5 ng/mL) for 30 min and then stained with anti-AMAP1 antibody, WGA and DAPI (n = 3). Scale bar = 50 μm. (c) Representative AMAP1 immunoblots of fractions from sucrose gradient centrifugation of HUVECs treated with or without IL-1β (2.5 ng/mL) for 30 min and the cumulative, quantitative densitometry data from three independent experiments are shown. Representative blots from three immunoprecipitation experiments using anti-AMAP1 (d) and anti-IKKβ (e) antibodies in HUVECs treated with or without IL-1β (2.5 ng/mL) for 30 min. The graph represents the cumulative, quantitative densitometry data of the IKKβ blot in anti-AMAP1 antibody precipitates (d), of the AMAP1 blot in anti-IKKβ antibody precipitates (e). Error bar: ±SD. * $P < 0.05$, *** $P < 0.005$ in a two-sided, Student's *t*-test. Full-length blots are presented in Supplementary Figure 4.

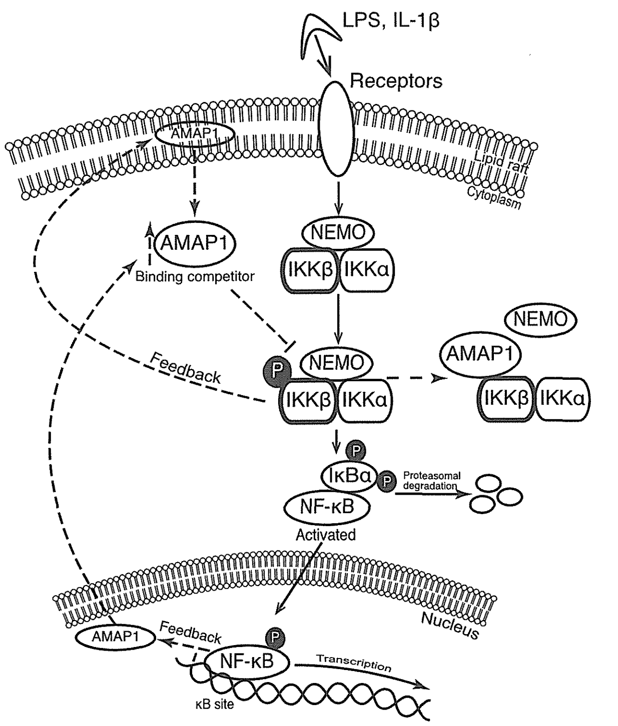

Figure 4 | Proposed model for AMAP1 as a binding protein of IKKβ and negative regulator of NF-κB. Dashed lines indicate the feedback mechanism.

radioresistance[7,9]. Considering the role of AMAP1 explored in this study, augmented expression of AMAP1 observed in cancer might indicate overwhelming NF-κB activation and self-repairing against cancer.

In summary, this study rediscovered AMAP1 as a negative regulator of NF-κB activity in a feedback mechanism, and AMAP1 could be a novel target for treatment or prevention against inflammatory diseases including cancer.

Methods

Reagents. The mammalian expression vectors that were used included pcDNA3.1-HA-AMAP1 and pcDNA3.1 as a control for AMAP1 overexpression, a series of mammalian expression vectors for IKKβ and its mutants (pIRES-AcGFP-hIKK2-WT, pIRES-AcGFP-hIKK2-Δ1, pIRES-AcGFP-hIKK2-Δ2, pIRES-AcGFP-hIKK2-Δ3 and pIRES-AcGFP-hIKK2-Δ4) and a series of mammalian expression vectors for AMAP1 and its mutants (pEBG/AMAP1-FL, pEBG/AMAP1-Bar, pEBG/AMAP1-PH, pEBG/AMAP1-ArfGAP, pEBG/AMAP1-ANK, pEBG/AMAP1-PRD and pEBG/AMAP1-SH3). The pcDNA3-HA-human-NEMO plasmid (Addgene plasmid 13512) to express NEMO was obtained from Professor Kunliang Guan (University of California, San Diego, USA)[34]. Small hairpin RNA (shRNA) expression constructs for silencing AMAP1 (shAMAP1) and control shRNA (shControl) were purchased from GeneCopoeia, Inc. (Rockville, MD, USA).

The antibodies that were used included anti-IKKβ (Millipore, Billerica, MA, USA); anti-AMAP1 (named anti-DDEF1, Santa Cruz Biotechnology, Dallas, Texas, USA); anti-HA (Sigma-Aldrich, St. Louis, MO, USA); monoclonal ANTI-FLAG® M2 (Sigma-Aldrich); a series of antibodies to anti-IKKβ, anti-phosphor-IκBα, anti-IκBα, anti-p65, anti-β-actin, anti-GAPDH, anti-TATA box-binding protein, anti-vimentin, anti-mouse IgG HRP-linked antibody and anti-rabbit IgG HRP-linked antibody (Cell Signaling Technology, Boston, MA, USA (CST)); anti-mouse IgG HRP and anti-rabbit IgG HRP (eBioscience, Inc. San Diego, CA, USA); Alexa Fluor 488 goat anti-rabbit IgG and Alexa Fluor 594 goat anti-mouse IgG (Invitrogen, Foster City, CA, USA); and Alexa Fluor 488 WGA. The reagents that were used included interleukin-1β (Wako Pure Chemical Industries, Ltd., Osaka, Japan (Wako)), LPS (Sigma-Aldrich) and NE-PER Nuclear and Cytoplasmic Extraction Reagents (Thermo Scientific, Rockford, IL, USA).

Cell culture. The human embryonic kidney 293T cell line (HEK293T) was maintained in DMEM (Wako) containing 10% FBS (Gibco, Foster City, CA, USA), 1% penicillin G/streptomycin (Sigma-Aldrich) at 37°C under 5% CO_2. Human umbilical vein endothelial cells (HUVECs) were maintained in Endothelial cell Basal Medium-2 (EBM-2) (Lonza, Basel, Switzerland) at 37°C under 5% CO_2.

Proteomics analysis. A Nano-LC/MALDI–TOF system was used with three types of IKKβ (wild-type IKKβ, a dominant-positive mutant of IKKβ and a dominant-negative mutant of IKKβ) that were overexpressed in HEK293T cells and immunoprecipitated by a specific antibody. Each sample was reduced with 45 mM of DTT (Wako), alkylated with 100 mM of iodoacetamide (Sigma-Aldrich) and digested with 2000 ng of trypsin (Promega, Madison, WI, USA). One-dimensional peptide fractionation was performed with a DiNa Direct Nano-Flow LC/MALDI system (KYA Tech., Tokyo, Japan) using a reverse-phase (RP) trap column (HiQ Sil C18-3, 0.8 mm i.d. × 3 mm) and an RP analytical column (HiQ Sil C18-3 Gradient, 0.15 mm i.d. × 50 mm). The peptides was subjected to the trap column and then to the analytical column using a gradient of 0–50% solvent B in solvent A over 65 minutes [solvent A: 0.1% trifluoroacetic Acid (TFA), 2% acetonitrile; solvent B: 0.1%TFA, 70% acetonitrile] followed by 50–100% solvent B for 15 minutes at a flow rate 200 nL/minute. The RP column eluent was spotted onto a MALDI sample plate using a DiNa Direct Nano-flow LC/MALDI system (KYA Tech.) and analyzed using a 4800 mass spectrometer (Applied Biosystems Inc., Foster City, CA, USA). The peptides were fragmented under collision-induced dissociation conditions to give fragment ions that produced sequence information for the peptide. The software packages used for data acquisition and analysis included GPS explorer (Applied Biosystems Inc.) and Mascot (Matrix Science, Boston, MA, USA), respectively. The parameters of tolerance for the searches were set to 100 ppm for the MS and 0.2 Da for the MS/MS analyses.

Co-immunoprecipitation (Co-IP). HEK293T cells (8×10^5) were cotransfected with 0.5 μg of AMAP1 plasmids and 0.5 μg of IKKβ plasmids using Effectene reagent (Qiagen, Valencia, CA, USA) according to the manufacturer's protocol. After 48 h, the cells were washed with PBS and lysed with Cell Lysis Buffer (CST). One milligram of the lysate was incubated with 1 μg of control IgG, anti-HA-tag or anti-FLAG antibody overnight at 4°C with agitation. Twenty-five microliters of protein G Sepharose (GE Healthcare, Uppsala, Sweden) was added, and the samples were rotated at 4°C for 1 h. The beads were washed three times with Cell Lysis Buffer and one time with Tris buffer pH 7.5. Proteins that were bound to the beads were eluted into SDS sample buffer, and the eluted material was analyzed by immunoblotting using anti-HA, anti-FLAG and anti-GST antibodies. Co-precipitation of endogenous AMAP1 with IKKβ was performed using anti-AMAP1 and anti-IKKβ antibodies.

Measurement of p65 activity. HEK293T cells were lysed with NE-PER Nuclear and Cytoplasmic Extraction Reagents (Thermo Scientific) for nuclear and cytoplasmic extractions. Transcription factor kits were used to detect the active NF-κB in the nuclear extract for NF-κB p65 according to the manufacturer's protocol. Briefly, the biotinylated NF-κB consensus sequence was bound to streptavidin-coated ELISA wells. Because only the active form of NF-κB (p65) binds to the DNA sequence, nonspecific binding was minimized. The p65 that was bound to the consensus sequence was incubated with anti-p65 antibody and then with a secondary, HRP-conjugated antibody. A chemiluminescent substrate was added to the wells, and the resulting signal was detected using a luminometer.

Sucrose gradient. Cells were treated with 5 ng/mL IL-1β or PBS for 30 min and lysed in cell lysis buffer (CST) containing 1 mM PMSF. An identical amount of protein from each sample was mixed with 90% sucrose in MES buffer (6 mL final volume, sucrose concentration 51.7–58.7%) and transferred to a Beckman ultracentrifuge tube. Four milliliters of 35% sucrose followed by 3 mL of 5% sucrose were overlaid, the samples were spun in a Beckman Coulter ultracentrifuge (39,000 rpm; approximately 180,000 × *g* in a SW40Ti rotor, 20 h), and 26 fractions were collected from the top of the gradient. For the detection of the lipid raft fractions, all fractions were dot-blotted with HRP-labeled cholera toxin B (Sigma-Aldrich) to detect Ganglioside GM1.

Immunofluorescence. HUVECs were grown on a 4-well chamber slide (Thermo Scientific) and treated with or without IL-1β 2.5 ng/mL for 30 min. The cells were washed with PBS, fixed with 4% paraformaldehyde and permeabilized with 0.5% Triton X-100. The cells were then incubated with blocking solution (5% goat normal serum in PBS) and labeled with anti-AMAP1 and anti-vimentin antibodies that were coupled to Alexa Fluor 488- and 584-conjugated secondary antibodies. The stained cells were mounted using Mounting Medium with DAPI (Vector Laboratories Inc., Burlingame, CA, USA). Images were captured and exported using a confocal microscope (Olympus FV1000; 60× oil-immersion lens, FLUOVIEW 3.0 software).

Statistical analysis. The data are presented as the mean of ±SD. Groups were compared using a two-tailed, Student's t-test. $P < 0.05$ was considered significant.

1. Oeckinghaus, A. & Ghosh, S. The NF-kappaB family of transcription factors and its regulation. *Cold Spring Harbor Perspect. Biol.* **1**, a000034, DOI:10.1101/cshperspect.a000034 (2009).
2. Karin, M. Nuclear factor-kappaB in cancer development and progression. *Nature* **441**, 431–436, DOI:10.1038/nature04870 (2006).

3. Rothwarf, D. M., Zandi, E., Natoli, G. & Karin, M. IKK-gamma is an essential regulatory subunit of the IkappaB kinase complex. *Nature* **395**, 297–300, DOI:10.1038/26261 (1998).
4. Mercurio, F. *et al.* IKK-1 and IKK-2: cytokine-activated IkappaB kinases essential for NF-kappaB activation. *Science* **278**, 860–866 (1997).
5. Li, Z. W. *et al.* The IKKbeta subunit of IkappaB kinase (IKK) is essential for nuclear factor kappaB activation and prevention of apoptosis. *J. Exp. Med.* **189**, 1839–1845 (1999).
6. Agarwal, A. *et al.* The AKT/I kappa B kinase pathway promotes angiogenic/ metastatic gene expression in colorectal cancer by activating nuclear factor-kappa B and beta-catenin. *Oncogene* **24**, 1021–1031, DOI:10.1038/sj.onc.1208296 (2005).
7. Karin, M. NF-kappaB as a critical link between inflammation and cancer. *Cold Spring Harbor Perspect. Biol.* **1**, a000141, DOI:10.1101/cshperspect.a000141 (2009).
8. Jiang, R. *et al.* High expression levels of IKKalpha and IKKbeta are necessary for the malignant properties of liver cancer. *Int. J. Cancer* **126**, 1263–1274, DOI:10.1002/ijc.24854 (2010).
9. Chaturvedi, M. M., Sung, B., Yadav, V. R., Kannappan, R. & Aggarwal, B. B. NF-kappaB addiction and its role in cancer: 'one size does not fit all'. *Oncogene* **30**, 1615–1630, DOI:10.1038/onc.2010.566 (2011).
10. Ashida, N. *et al.* IKKbeta regulates essential functions of the vascular endothelium through kinase-dependent and -independent pathways. *Nat. Commun.* **2**, 318, DOI:10.1038/ncomms1317 (2011).
11. Furman, C., Short, S. M., Subramanian, R. R., Zetter, B. R. & Roberts, T. M. DEF-1/ ASAP1 is a GTPase-activating protein (GAP) for ARF1 that enhances cell motility through a GAP-dependent mechanism. *J. Biol. Chem.* **277**, 7962–7969, DOI:10.1074/jbc.M109149200 (2002).
12. Inoue, H., Ha, V. L., Prekeris, R. & Randazzo, P. A. Arf GTPase-activating protein ASAP1 interacts with Rab11 effector FIP3 and regulates pericentrosomal localization of transferrin receptor-positive recycling endosome. *Mol. Biol. Cell.* **19**, 4224–4237, DOI:10.1091/mbc.E08-03-0290 (2008).
13. Liu, Y., Yerushalmi, G. M., Grigera, P. R. & Parsons, J. T. Mislocalization or reduced expression of Arf GTPase-activating protein ASAP1 inhibits cell spreading and migration by influencing Arf1 GTPase cycling. *J. Biol. Chem.* **280**, 8884–8892, DOI:10.1074/jbc.M412200200 (2005).
14. Randazzo, P. A. *et al.* The Arf GTPase-activating protein ASAP1 regulates the actin cytoskeleton. *Proc. Natl. Acad. Sci. U. S. A.* **97**, 4011–4016, DOI:10.1073/ pnas.070552297 (2000).
15. Nam, J. M. *et al.* CIN85, a Cbl-interacting protein, is a component of AMAP1-mediated breast cancer invasion machinery. *Embo J.* **26**, 647–656, DOI:10.1038/ sj.emboj.7601534 (2007).
16. Muller, T. *et al.* ASAP1 promotes tumor cell motility and invasiveness, stimulates metastasis formation in vivo, and correlates with poor survival in colorectal cancer patients. *Oncogene* **29**, 2393–2403, DOI:10.1038/onc.2010.6 (2010).
17. Onodera, Y. *et al.* Rab5c promotes AMAP1-PRKD2 complex formation to enhance beta1 integrin recycling in EGF-induced cancer invasion. *J. Cell. Biol.* **197**, 983–996, DOI:10.1083/jcb.201201065 (2012).
18. Hashimoto, S. *et al.* Requirement for Arf6 in breast cancer invasive activities. *Proc. Natl. Acad. Sci. U. S. A.* **101**, 6647–6652, DOI:10.1073/pnas.0401753101 (2004).
19. Onodera, Y. *et al.* Expression of AMAP1, an ArfGAP, provides novel targets to inhibit breast cancer invasive activities. *Embo J.* **24**, 963–973, DOI: 10.1038/ sj.emboj.7600588 (2005).
20. Sabe, H., Onodera, Y., Mazaki, Y. & Hashimoto, S. ArfGAP family proteins in cell adhesion, migration and tumor invasion. *Curr. Opin. Cell. Biol.* **18**, 558–564, DOI:10.1016/j.ceb.2006.08.002 (2006).
21. Morishige, M. *et al.* GEP100 links epidermal growth factor receptor signalling to Arf6 activation to induce breast cancer invasion. *Nat. Cell. Biol.* **10**, 85–92, DOI:10.1038/ncb1672 (2008).
22. Boulay, P. L., Cotton, M., Melancon, P. & Claing, A. ADP-ribosylation factor 1 controls the activation of the phosphatidylinositol 3-kinase pathway to regulate epidermal growth factor-dependent growth and migration of breast cancer cells. *J. Biol. Chem.* **283**, 36425–36434, DOI:10.1074/jbc.M803603200 (2008).
23. Haque, A. *et al.* An ADP ribosylation factor-GTPase activating protein negatively regulates the production of proinflammatory mediators in response to lipopolysaccharide. *Cancer Immunol. Immunother.* **60**, 1439–1446, DOI:10.1007/ s00262-011-1048-9 (2011).
24. Sabe, H. *et al.* The EGFR-GEP100-Arf6-AMAP1 signaling pathway specific to breast cancer invasion and metastasis. *Traffic* **10**, 982–993, DOI:10.1111/ j.1600-0854.2009.00917.x (2009).
25. Xu, G. *et al.* Crystal structure of inhibitor of kappaB kinase beta. *Nature* **472**, 325–330, DOI:10.1038/nature09853 (2011).
26. May, M. J. *et al.* Selective inhibition of NF-kappaB activation by a peptide that blocks the interaction of NEMO with the IkappaB kinase complex. *Science* (New York, N.Y.) **289**, 1550–1554 (2000).
27. Lin, D. *et al.* ASAP1, a gene at 8q24, is associated with prostate cancer metastasis. *Cancer Res.* **68**, 4352–4359, DOI:10.1158/0008-5472.CAN-07-5237 (2008).
28. Birbach, A. *et al.* Signaling molecules of the NF-kappa B pathway shuttle constitutively between cytoplasm and nucleus. *J. Biol. Chem.* **277**, 10842–10851, DOI:10.1074/jbc.M112475200 (2002).
29. Verma, U. N., Yamamoto, Y., Prajapati, S. & Gaynor, R. B. Nuclear role of I kappa B Kinase-gamma/NF-kappa B essential modulator (IKK gamma/NEMO) in NF-kappa B-dependent gene expression. *J. Biol. Chem.* **279**, 3509–3515, DOI:10.1074/ jbc.M309300200 (2004).
30. de Martin, R. *et al.* Cytokine-inducible expression in endothelial cells of an I kappa B alpha-like gene is regulated by NF kappa B. *Embo J.* **12**, 2773–2779 (1993).
31. Haskill, S. *et al.* Characterization of an immediate-early gene induced in adherent monocytes that encodes I kappa B-like activity. *Cell* **65**, 1281–1289 (1991).
32. Sun, S. C., Ganchi, P. A., Ballard, D. W. & Greene, W. C. NF-kappa B controls expression of inhibitor I kappa B alpha: evidence for an inducible autoregulatory pathway. *Science* (New York, N.Y.) **259**, 1912–1915 (1993).
33. Pahl, H. L. Activators and target genes of Rel/NF-kappaB transcription factors. *Oncogene* **18**, 6853–6866, DOI:10.1038/sj.onc.1203239 (1999).
34. Tang, E. D. Negative Regulation of the Forkhead Transcription Factor FKHR by Akt. *J. Biol. Chem.* **274**, 16741–16746, DOI:10.1074/jbc.274.24.16741 (1999).

Acknowledgments

This work was performed under the Sponsored Research Program contracted between Kyoto University and Otsuka Pharmaceutical Co., Ltd., and was also supported by a Grant-in-Aid for Scientific Research from the Ministry of Education, Culture, Sports, Science and Technology of Japan. We also thank Prof. Kunliang Guan for the pcDNA3-HA-human-NEMO plasmid.

Author contributions

D.N.-T. and N.A. conceived and designed the research. D.N.-T., M.K., A.Y. and N.A. performed the experiments. A.Y. and A.H. made the constructs of AMAP1. H.S., E.N., K.K., H.A., T.K., T.K. and M.Y. supervised the project.

Additional information

Supplementary information accompanies this paper at http://www.nature.com/ scientificreports

Competing financial interests: The authors declare no competing financial interests.

How to cite this article: Nguyen Tien, D. *et al.* AMAP1 as a negative-feedback regulator of nuclear factor-κB under inflammatory conditions. *Sci. Rep.* **4**, 5094; DOI:10.1038/ srep05094 (2014).

SCIENTIFIC REPORTS

OPEN

SUBJECT AREAS:
EXPERIMENTAL MODELS OF DISEASE
MIRNAS

Received
20 March 2014

Accepted
30 May 2014

Published
16 June 2014

Correspondence and requests for materials should be addressed to K.O. (kohono@kuhp.kyoto-u.ac.jp)

* These authors contributed equally to this work.

MicroRNA-33b knock-in mice for an intron of sterol regulatory element-binding factor 1 (*Srebf1*) exhibit reduced HDL-C *in vivo*

Takahiro Horie[1,2]*, Tomohiro Nishino[1]*, Osamu Baba[1], Yasuhide Kuwabara[1], Tetsushi Nakao[1], Masataka Nishiga[1], Shunsuke Usami[1], Masayasu Izuhara[1], Fumiko Nakazeki[1], Yuya Ide[1], Satoshi Koyama[1], Naoya Sowa[1], Naoya Yahagi[3], Hitoshi Shimano[3], Tomoyuki Nakamura[4], Koji Hasegawa[5], Noriaki Kume[6], Masayuki Yokode[2], Toru Kita[7], Takeshi Kimura[1] & Koh Ono[1]

[1]Department of Cardiovascular Medicine, Graduate School of Medicine, Kyoto University, Kyoto 606-8507, Japan, [2]Department of Clinical Innovative Medicine, Institute for Advancement of Clinical and Translational Science, Graduate School of Medicine, Kyoto University, Kyoto 606-8507, Japan, [3]Department of Internal Medicine (Endocrinology and Metabolism), Graduate School of Comprehensive Human Sciences, Nutrigenomics Research Group, Faculty of Medicine, and International Institute for Integrative Sleep Medicine (IIIS), World Premir International Research Center Initiative (WPI), University of Tsukuba, 1-1-1 Tennodai, Tsukuba, Ibaraki 305-8575, Japan, [4]Department of Pharmacology, Kansai Medical University, Moriguchi, Osaka 570-8506, Japan, [5]Division of Translational Research, National Hospital Organization, Kyoto Medical Center, Kyoto 612-8555, Japan, [6]Division of Clinical Pharmacy, Faculty of Pharmaceutical Sciences, Kobe Gakuin University, Kobe 650-8586, Japan, [7]Department of Cardiovascular Medicine, Kobe City Medical Center General Hospital, Kobe 650-0046, Japan.

MicroRNAs (miRs) are small non-protein-coding RNAs that bind to specific mRNAs and inhibit translation or promote mRNA degradation. Recent reports, including ours, indicated that miR-33a located within the intron of sterol regulatory element-binding protein (SREBP) 2 controls cholesterol homeostasis and can be a possible therapeutic target for treating atherosclerosis. Primates, but not rodents, express miR-33b from an intron of *SREBF1*. Therefore, humanized mice, in which a miR-33b transgene is inserted within a *Srebf1* intron, are required to address its function *in vivo*. We successfully established miR-33b knock-in (KI) mice and found that protein levels of known miR-33a target genes, such as ABCA1, ABCG1, and SREBP-1, were reduced compared with those in wild-type mice. As a consequence, macrophages from the miR-33b KI mice had a reduced cholesterol efflux capacity via apoA-I and HDL-C. Moreover, HDL-C levels were reduced by almost 35% even in miR-33b KI hetero mice compared with the control mice. These results indicate that miR-33b may account for lower HDL-C levels in humans than those in mice and that miR-33b is possibly utilized for a feedback mechanism to regulate its host gene *SREBF1*. Our mice will also aid in elucidating the roles of miR-33a/b in different genetic disease models.

Sterol regulatory element-binding proteins (SREBPs) comprise a subclass of basic helix-loop-helix leucine zipper transcription factors conserved from yeasts to humans and regulate the expression of genes required for maintaining cellular lipid homeostasis[1]. Mammals possess two SREBP genes, SREBP-1 and SREBP-2 (known as *SREBF1* and *SREBF2*, respectively) that express three major SREBP proteins. Two SREBP-1 isoforms, SREBP-1a and SREBP-1c, primarily regulate fatty acid metabolism, and SREBP-2 is the main regulator of cholesterol metabolism, although there is some functional overlap among the three SREBP isoforms[2–4].

MicroRNAs (miRs) are small non-protein-coding RNAs that bind to specific mRNAs and inhibit translation or promote mRNA degradation[5]. Recent advances in the understanding of miR biology revealed that the genetic loci encoding for the transcription factors SREBP-1 and SREBP-2 also encode for the miRs miR-33b and miR-33a, respectively. Recent reports, including ours, indicated that miR-33a controls ABCA1 expression and reduces HDL-C levels[6–8] and that miR-33a deficiency ameliorates atherosclerosis in mice[9–11]. However, in rodents, a part of miR-33b is lacking from a *Srebf1* intron (Supplementary Fig. 1a), and it is impossible to determine the precise coordinate mechanisms of miR-33a and miR-33b; the expression of these miR-33s is expected to depend on their corresponding host genes. Of note, SREBP-1 and SREBP-2 are differentially regulated by hormones, dietary challenges, or statin treatment, and the amounts and functions of miR-33a and miR-33b would be greatly affected under these conditions.

miR-33a and miR-33b are identical in their seed sequences, and thus have been predicted to repress the same set of genes with similar specificities. Antisense oligonucleotides against miR-33a are believed to simultaneously target miR-33a and miR-33b. However, there remains a 2-nucleotide mismatch after the seed sequence between miR-33a and miR-33b (Supplementary Fig. 1a), and whether this difference results in differential targeting remains to be established. Moreover, some of the previously established miR-33a target genes were not dysregulated in our miR-33a-deficient mice. Therefore, humanized mice, in which a miR-33b transgene is inserted within a *Srebf1* intron, are required to address its function *in vivo*.

We successfully established miR-33b knock-in (KI) mice for the same intron as in humans. The protein levels of known miR-33a target genes, such as ABCA1, ABCG1, and SREBP-1, were reduced under basal conditions. An LXR agonist, which induces *Srebf1* expression, enhanced miR-33b production. *In vitro* experiments indicated that macrophages from the miR-33b KI mice had a reduced cholesterol efflux capacity via apoA-I and HDL-C. Moreover, HDL-C levels were reduced by almost 35% even in miR-33b KI hetero mice compared with the control mice.

The feasibility of genetic manipulation is one of the many advantages of using mice as a model organism. However, the lack of miR-33b in mouse *Srebf1* has raised an important concern regarding the direct translation of data from rodent models to human physiology and metabolic disorders. Our mice will aid in answering these questions and will be useful for assessing the risks and benefits of long-term alterations in miR-33s in different disease models. These mice might also be useful for screening of the drugs that alter the levels of miR-33a and miR-33b.

Results

miR-33b is co-expressed with *SREBF1* in the human cell line HepG2. It is assumed that a miR located within an intron of a gene is expressed along with its host gene and exerts its specific function[12]. Because miR-33b is located in a *SREBF1* intron in humans (Supplementary Fig. S1a), we stimulated human cell line HepG2 with the LXR agonist T0901317 and determined miR-33b and miR-33a expression along with the expression of the host genes *SREBF1* and *SREBF2*. As shown in Fig. 1a and b, miR-33b expression seemed to tag along behind *SREBF1* expression. In contrast, miR-33a and *SREBF2* expression was not affected by LXR stimulation (Fig. 1c and d).

Generation of miR-33b KI mice. Because miR-33b is located in *SREBF1* intron 16 in humans and there are high homologies in exons 16 and 17 between human and mouse (82.6% of nucleotides and 79.7% of amino acids, Supplementary Fig. S1b), we introduced the human miR-33b sequence into intron 16 of mouse *Srebf1*. We isolated and amplified the region that encoded for the complete pre-miR sequence of human miR-33b and adjacent sequence, which enabled the introduction of miR-33b into intron 16 of mouse *Srebf1* (Fig. 2a). Supplementary Figure S2a and Figure 2b show the results of Southern blotting analysis of genomic DNA from ES cells and tail genomic DNA from F1 mice that were successfully targeted by a KI vector, respectively. PCR analysis indicated the specific patterns for wild-type (WT), $KI^{+/-}$, and $KI^{+/+}$ mice (Fig. 2c). This miR-33b KI strategy did not alter *Srebf1* intron 16 splicing, as confirmed by PCR (Fig. 2d) and sequencing (Fig. 2e). The expression levels of miR-33b in miR-33b $KI^{+/-}$ mice were almost half of those in miR-33b $KI^{+/+}$ mice (Fig. 2f). We also measured the levels of miR-33b, miR-33a, *Srebf1*, and *Srebf2* in WT and KI mice in both the liver and the peritoneal macrophages (Supplementary Figure S2b–d and S3a–d). *Srebf1* levels were similar among these mice (Supplementary Figure S2c and S3c). Although there was no difference in miR-33a levels in macrophages (Supplementary Figure S3b), miR-33a levels were increased in proportion of the expression levels of miR-33b in the liver (Supplementary Figure S2b). The miR-33b $KI^{+/+}$ mice were born with the expected Mendelian ratios, were viable, fertile, and did not exhibit any obvious abnormalities in size, shape, or structure up to 8 weeks of age. Relative tissue expression pattern of miR-33b was similar to that of *Srebf1* (Supplementary Fig. S2e and S2f).

miR-33b is upregulated after inducing *Srebf1* expression. We next sought to confirm whether miR-33b expression was affected by endogenous changes in *Srebf1* expression by the LXR agonist T0901317[13]. When primary hepatocytes from the miR-33b $KI^{+/+}$ mice were stimulated with T0901317, *Srebf1* and miR-33b mRNA levels were significantly increased in parallel, although this increase was faster for *Serbf1* than for miR-33b (Fig. 3a and b). To check this effect *in vivo*, T0901317 was suspended in 0.5% carboxymethyl-cellulose and administrated to 8-week-old male miR-33b $KI^{+/+}$ mice at a dose of 25 mg/kg for 3 days. The average liver weight of the T0901317-treated mice was 1.5-fold greater than that of the control mice (Supplementary Fig. S4a). *Srebf1* and miR-33b expression levels in the liver were also significantly increased in parallel (Fig. 3c and d). The average liver weight and *Srebf1* expression level in the liver of T0901317-treated WT mice were shown in Supplementary Figure S4b and S4c. These results indicate that miR-33b was co-expressed with *Srebf1* in the livers of the T0901317-treated miR-33b KI mice.

miR-33b KI results in alterations in miR-33a target proteins ABCA1 and SREBP-1. We determined ABCA1, SREBP-1, CPT1a, and AMPKα protein levels in the liver (Fig. 4a and Supplementary

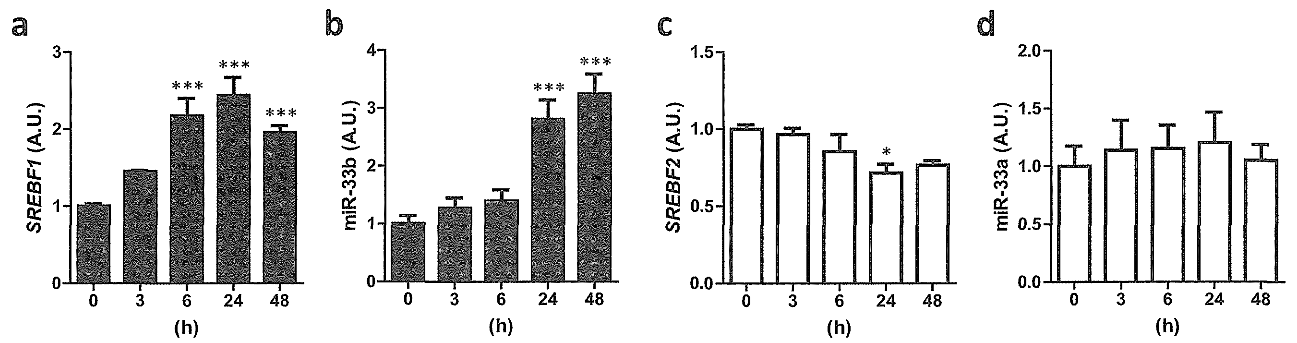

Figure 1 | miR-33b is co-expressed with *SREBF1* in HepG2 cells. HepG2 cells were treated with T0901317 (10 μM) for the indicated time. The relative expressions of *SREBF1* (a), miR-33b (b), *SREBF2* (c), and miR-33a (d) are shown (n = 6–9). Values are mean ± s.e.m. *$p < 0.05$, ***$p < 0.001$ compared with 0 h.

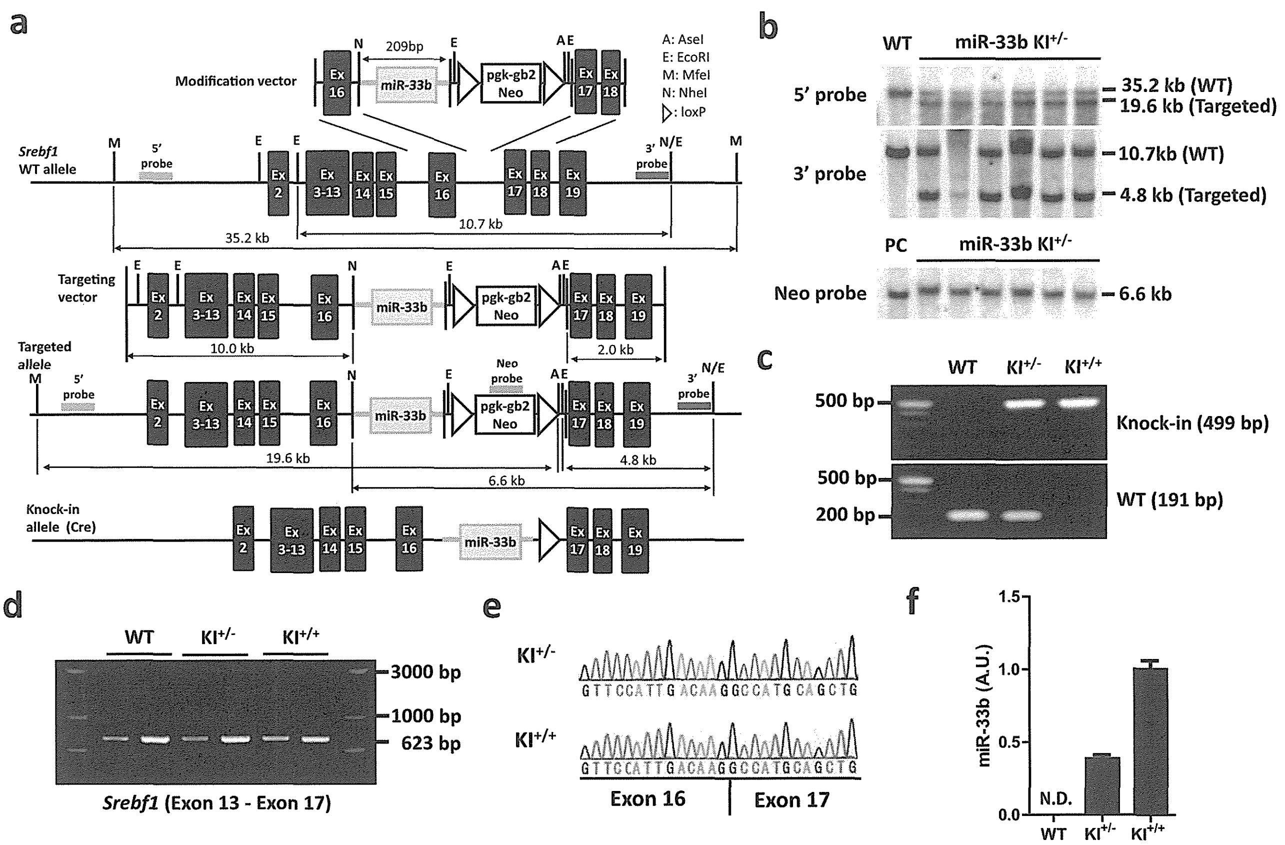

Figure 2 | Generation of miR-33b knock-in (KI) mice. (a). Strategy used to generate miR-33b KI mice. (b). Southern blotting of mouse tail genomic DNA. Representative images are shown. (c). PCR analysis of mouse tail genomic DNA. Representative images are shown. (d). RT-PCR analysis of *Srebf1* expression in the livers of 8-week-old mice. Sense primer was designed for exon 13, and antisense primer was designed for exon17. Note that there was no other band except for that of the correct size. Representative images are shown. (e). Sequencing alignment at the joint between exons 16 and 17 of *Srebf1* in the indicated mice. (f). Relative expression of miR-33b in the livers of 8-week-old mice (n = 6). N.D., not determined. Values are mean ± s.e.m.

Figure S5). As shown in Fig. 4a, Supplementary Figure S5a, and S5b, ABCA1 and SREBP-1 protein levels were lower in the livers of the miR-33b KI mice. However, the protein levels of some of the previously defined miR-33a target genes, such as CPT1a and AMPKα remained unchanged. We also analyzed protein expressions of glucose metabolic genes (Fig. 4b and Supplementary

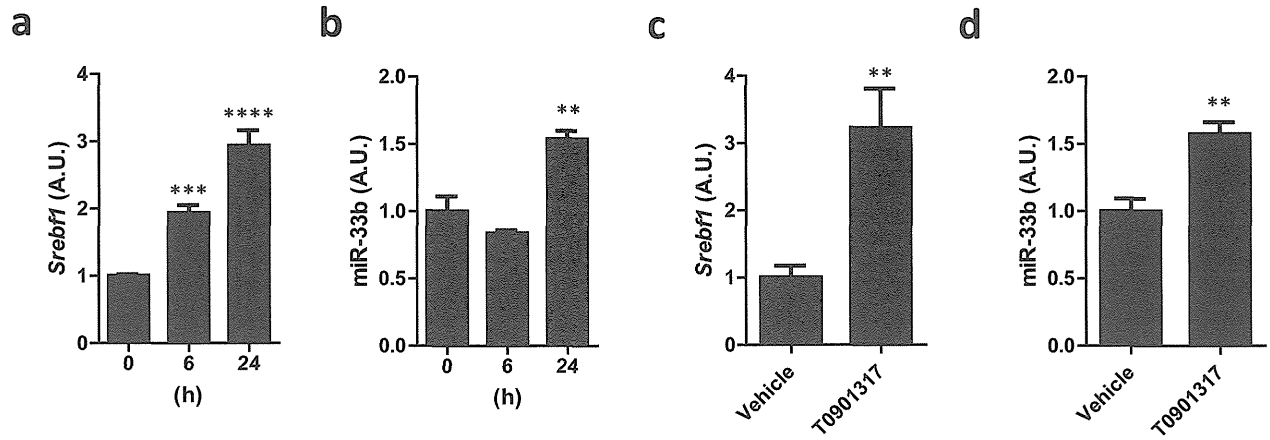

Figure 3 | miR-33b is co-expressed with *Srebf1* in miR-33b KI mice. (a). Relative *Srebf1* expression levels in primary hepatocytes from miR-33b KI$^{+/+}$ mice treated with T0901317 (10 μM) for the indicated time. Values are mean ± s.e.m (n = 6). **p < 0.01 ***p < 0.001 by one-way analysis of variance. (b). Relative miR-33b expression levels in primary hepatocytes from miR-33b KI$^{+/+}$ mice treated with T0901317 (10 μM) for the indicated time. Values are mean ± s.e.m (n = 6). **p < 0.01 by one-way analysis of variance. (c). Relative *Srebf1* expression levels in the livers of 8-week-old male miR-33b KI$^{+/+}$ mice treated with T0901317 (25 mg/kg) for 3 days. Values are means ± s.e.m (n = 6). **p < 0.01 compared with the vehicle. (d). Relative miR-33b expression levels in the livers of 8-week-old male miR-33b KI$^{+/+}$ mice treated with T0901317 (25 mg/kg) for 3 days. Values are mean ± s.e.m (n = 6). *p < 0.05 compared with the vehicle.

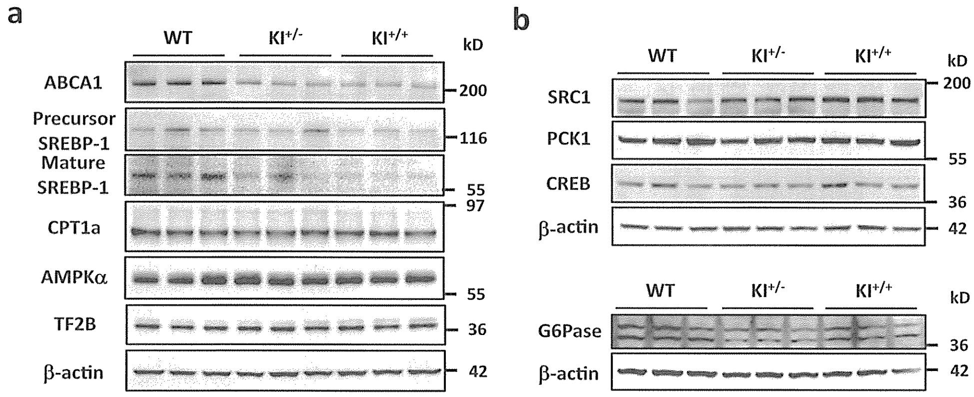

Figure 4 | miR-33b regulates ABCA1 and SREBP-1. (a). Western blotting analysis for ABCA1, SREBP-1, CPT1a, and AMPKα protein levels in the livers of WT, $KI^{+/-}$, and $KI^{+/+}$ mice. Representative images are shown. TF2B and β-actin were used as loading controls. (b). Western blotting analysis for SRC1, PCK1, CREB and G6Pase protein levels in the livers of WT, $KI^{+/-}$, and $KI^{+/+}$ mice. Representative images are shown. β-actin were used as loading controls.

Figure S5c–f). However, no significant change in protein level was observed in PCK1, G6PC, and CREB in the liver of miR-33b KI mice compared with that of control mice. SRC1 was up-regulated in miR-33bKI mice and it was opposite to the results of previous report[14].

miR-33b KI reduces cholesterol efflux in macrophages. To investigate a physiological role of miR-33b in mice, we first compared the functions of peritoneal macrophages from the WT and miR-33b $KI^{+/+}$ mice. ABCA1 and ABCG1 protein levels were lower in macrophages from the miR-33b $KI^{+/+}$ mice than from the WT mice (Fig. 5a and Supplementary Figure S3e and S3f), which was compatible with the findings for our miR-33a-deficient mice. We determined apoA-I- and HDL-C-mediated cholesterol efflux from peritoneal macrophages and found that macrophages from the miR-33b $KI^{+/+}$ mice had lower apoA-I- and HDL-C-mediated cholesterol efflux than those from the WT mice (Fig. 5b).

A single miR-33b copy reduces serum HDL levels. Hepatic ABCA1 overexpression increases HDL-C levels[15], and liver-specific deletion of ABCA1 results in a substantial decrease in plasma HDL-C levels (approximately 80%) in chow-fed mice[16]. Moreover, we previously reported that the miR-$33a^{-/-}$ mice had 22%–39% higher serum HDL-C levels than the WT mice[8]. Thus, we determined the serum HDL-C levels of the WT, miR-33b $KI^{+/-}$, and miR-33b $KI^{+/+}$ mice at the age of 8 weeks.

Serum HDL-C levels were significantly decreased in the miR-33b $KI^{+/-}$ and miR-33b $KI^{+/+}$ mice compared with the WT mice (Table). We also classified and quantified serum lipoproteins using high-performance liquid chromatography (HPLC). Mean plots of the HPLC elution profile of serum from male mice are shown in Fig. 5c, and the lipid profiles are summarized in Supplementary Table S1. These results show that only one copy of miR-33b was sufficient to substantially reduce HDL-C and total cholesterol to the same levels as those in the miR-33b $KI^{+/+}$ mice. Moreover, the decreased HDL levels mainly comprised very large-, large-, and medium-sized HDLs (mature HDLs) (Fig. 5c and Supplementary Table S1).

Discussion

In the present study, we successfully established humanized mice, in which a miR-33b transgene was inserted within the same intron as that in human *SREBF1*. The LXR agonist T0901317, which is a well-established *Srebf1* expression inducer, enhanced miR-33b production. The protein levels of known miR-33a/b target genes, such as ABCA1, ABCG1, and SREBP-1, were reduced under basal conditions. *In vitro* experiments indicated that macrophages from the miR-33b $KI^{+/+}$ mice had a reduced cholesterol efflux capacity via apoA-I and HDL-C. Finally, HDL-C levels were reduced by almost 35% even in the miR-33b $KI^{+/-}$ mice compared with the WT mice without any changes in triglyceride (TG) levels.

In contrast to humans and other mammals, rodents lack miR-33b and only have miR-33a in *Srebf2*. This needs to be kept in mind when attempting to directly translate to humans the previous results that miR-33a inhibition could prevent atherosclerosis in mouse models because of two reasons. First, *SREBF1* and *SREBF2* are differentially regulated by hormones, dietary challenges, and lipid-lowering agents, including statins[17]. This indicates that both isoforms of miR-33 participate in regulating the primary risk factors of metabolic syndrome, which accelerate atherosclerosis. Second, miR-33b differs from miR-33a by 2-nucleotides and may have a different target profile, including stronger effects on targets in the SREBP-1-dependent regulation of fatty acid/TG homeostasis and insulin signaling. We found increased miR-33b expression after treatment with LXR agonist in our mice, which indicated that miR-33b was co-expressed with its *Srebf1* host gene and enabled us to study the impact of *Srebf1*-derived miR-33b on cholesterol/lipid homeostasis.

We have not yet succeeded in identifying miR-33b-specific target genes. Even previously reported miR-33b target genes were not reduced in the liver of miR-33b KI mice compared with that of control mice. One of the reasons of such result may be that the previous study was conducted in human cell line and potential binding sites of miR-33b are not conserved at least in PCK1 3′UTR of mice. It is also possible that some compensated mechanisms may have occurred in miR-33b KI mice. However, the protein levels of miR-33a target genes, such as ABCA1, ABCG1, and SREBP-1, were reduced[18]. Moreover, the protein levels of previously defined miR-33a target genes, which were not dysregulated in miR-33a KO mice, including CPT1a and AMPKα, remained unchanged[19,20]. Thus, it may be necessary to assess those conditions when *Srebf1* expression is strongly affected to establish the importance of the functions of miR-33b. In any event, the numbers of miR-33b transcripts were greater than those of miR-33a transcripts, and this underscores the importance of miR-33b[21]. Although there were no differences in the levels of miR-33a in macrophages, it is interesting that the levels of miR-33a were increased in proportion to the expression levels of miR-33b in the liver. Because *Srebf1* level is higher in the liver than that in macrophages[22], it is possible that miR-33b and miR-33a compete for the same target gene binding sites in the liver, and that the degradation of miR-33a is inhibited by miR-33b expression. In addition, there may be other unknown mechanisms.

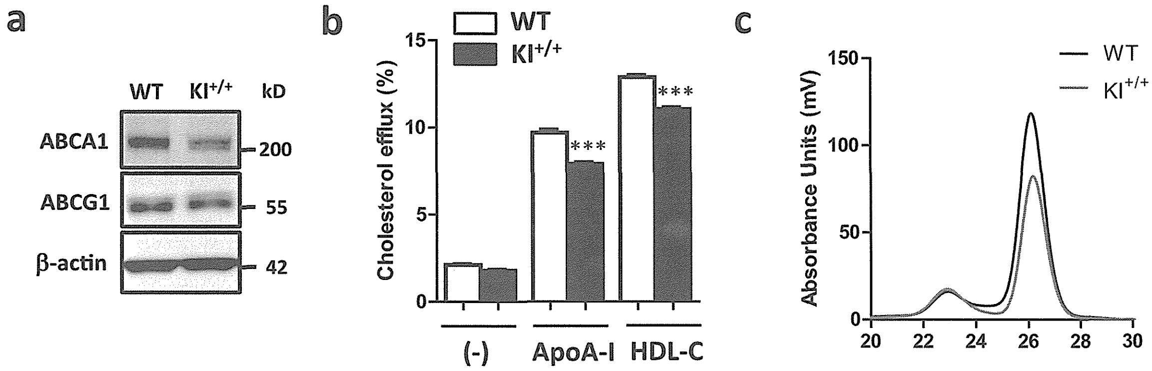

Figure 5 | miR-33b reduces cellular cholesterol efflux and serum HDL-C levels. (a). Western blotting for ABCA1 and ABCG1 proteins in peritoneal macrophages from WT and $KI^{+/+}$ mice. Representative images are shown. β-actin was used as the loading control. (b). Cholesterol efflux to apoA-I and HDL-C in peritoneal macrophages from WT and $KI^{+/+}$ mice (n = 6 each). Values are mean ± s.e.m. ***$p < 0.001$ (c). Mean plots of HPLC analysis for serum cholesterol in WT and $KI^{+/+}$ mice (n = 4 and 5, respectively).

miRs are known to target long non-coding RNAs whose functions are largely unknown, and interactions between miRs are also possible[23]. Thus, miR-33b-specific functions should be determined in future experiments.

Rayner *et al.* recently showed that inhibiting miR-33a and miR-33b in healthy male non-human primates increased circulating HDL-C levels[21]. More recently, Rottiers *et al.* reported that miR-33a and miR-33b acted in a redundant manner and that inhibiting both isoforms by an 8-mer LNA-modified anti-miR enhanced HDL-C levels[24]. Our data demonstrated that miR-33b indeed functions to control HDL-C levels, which highlights the importance of targeting both miR-33 family members simultaneously. It is noteworthy that only one copy of miR-33b (miR-33b $KI^{+/-}$ mice) significantly reduced HDL-C levels to the same levels as those in the miR-33b $KI^{+/+}$ mice. This explains one of the reasons why human HDL-C levels are lower than those of mice and indicates that it is important to considerably reduce miR-33b levels if pharmacological targeting of miR-33s is used to increase HDL-C levels. In this context, the current LNA-modified anti-miR technique is quite potent for reducing the levels of both miR-33 isoforms and may be useful for anti-atherosclerosis therapy.

In addition to the effects on HDL-C, a study by Rayner *et al.* showed that miR-33 antagonism reduced very low-density lipoprotein-associated TGs in their cohort of normal male African green monkeys[21]. However, Rottiers *et al.* did not find any significant changes in TG levels when using miR-33a/b-targeting LNA-anti-miR treatment[24]. In our present miR-33b KI study and in previous miR-33a KO experiments[8], we did not observe any changes in TG levels, indicating that modulation of miR-33s is unlikely to have a strong effect on TG levels, although species differences and different dietary conditions need to be considered.

In contrast, we found a significant inhibitory effect of miR-33b on SREBP-1. A feedback system of SREBP-2 by cholesterol levels is well known, which maintains appropriate levels of cellular cholesterol.

Table | Serum profiling of WT, $KI^{+/-}$, and $KI^{+/+}$ mice

	WT (n = 4)	$KI^{+/-}$ (n = 4)		$KI^{+/+}$ (n = 4)	
TP (g/dL)	4.375 ± 0.1109	4.275 ± 0.04787		4.350 ± 0.05000	
ALB (g/dL)	2.950 ± 0.1190	2.825 ± 0.1109		2.900 ± 0.04082	
BUN (mg/dL)	21.75 ± 0.6801	20.58 ± 1.248		21.58 ± 1.680	
CRE (mg/dL)	0.1125 ± 0.002500	0.0925 ± 0.004787	*	0.0975 ± 0.006292	
Na (mEq/L)	152.5 ± 0.6455	153.5 ± 0.2887		153.8 ± 0.4787	
K (mEq/L)	3.350 ± 0.05000	3.325 ± 0.0750		3.350 ± 0.1041	
Cl (mEq/L)	110.5 ± 0.6455	110.8 ± 0.2500		111.0 ± 0.5774	
Ca (mg/dL)	8.500 ± 0.1871	8.325 ± 0.1109		8.350 ± 0.08660	
IP (mg/dL)	7.775 ± 0.4589	7.225 ± 0.2955		7.400 ± 0.4637	
T-BIL (mg/dL)	0.0875 ± 0.004787	0.0925 ± 0.008539		0.0825 ± 0.01109	
AST (IU/L)	39.25 ± 1.702	33.50 ± 1.658		39.25 ± 1.702	
ALT (IU/L)	26.50 ± 3.663	21.00 ± 2.415		22.75 ± 1.702	
ALP (IU/L)	505.5 ± 48.55	398.5 ± 40.01		480.0 ± 29.31	
LDH (IU/L)	278.3 ± 77.21	243.5 ± 55.30		255.0 ± 55.26	
AMY (IU/L)	2295 ± 68.22	2224 ± 62.39		2363 ± 97.02	
γ-GTP (IU/L)	3>	3>		3>	
T-CHO (mg/dL)	98.50 ± 5.694	66.25 ± 2.287	**	62.00 ± 1.225	***
TG (mg/dL)	34.75 ± 2.780	32.25 ± 3.065		35.25 ± 4.328	
NEFA (μEq/L)	471.0 ± 47.36	474.8 ± 71.81		459.5 ± 55.01	
LDL-C (mg/dL)	6.750 ± 0.6292	6.750 ± 0.6292		6.000 ± 0.0	
HDL-C (mg/dL)	57.75 ± 4.171	39.25 ± 0.7500	**	37.25 ± 0.6292	**
GLU (mg/dL)	216.3 ± 22.98	180.5 ± 8.930		197.8 ± 11.92	

Values are mean ± s.e.m. Blood was obtained from chow-fed 8-wk-old male mice after 4 h fasting.
*$p < 0.05$;
**$p < 0.01$;
***$p < 0.001$ compared with WT mice.

However, a similar mechanism has not been established for SREBP-1. Chronic activation of SREBP-1c in cases of overnutrition can lead to serious obesity-related problems. miR-33b may be utilized for a feedback mechanism to regulate its host gene *SREBF1* because insulin induces hepatic SREBP-1c expression and promotes lipogenesis and hepatic TG synthesis (Supplementary Fig. S6).

In the present study, we demonstrated the effect of miR-33b on HDL-C levels *in vivo*. We assume that inhibiting both miR-33a and miR-33b will have a significant effect on HDL-C levels in clinical settings. However, it is known that one miR can have hundreds of target genes and unexpected side effects may occur due to long-term therapeutic modulation of miR-33 to cure metabolic diseases. Careful observations of miR-33b KI and miR-33a-deficient mice and intercrossing of these mice will enable us to detect miR-33a- and miR-33b-specific target genes and to elucidate the overall functions of miR-33a and miR-33b *in vivo*. Moreover, our mice will aid in analyzing the roles of miR-33a/b in different genetic disease models and in screening drug candidates that can modulate miR-33a and miR-33b levels and activities.

Methods

Materials. The following antibodies were used: anti-ABCA1 (NB400-105) and anti-ABCG1 (NB400-132) (Novus Biologicals, Littleton, CO, USA); anti-AMPKα (#2532) and anti-CREB (#9197) (Cell Signaling Technology, Beverly, MA, USA); anti-CPT1a (ab128568) and anti-PCK1 (ab70358) (Abcam, Cambridge, UK); anti-β-actin (AC-15; A5441, Sigma-Aldrich, St. Louis, MO, USA); anti-SREBP-1 (sc-13551, sc-8984), anti-SRC1 (sc-8995), anti-G6Pase (sc-27198), and anti-TF2B (sc-225) (Santa Cruz, Biotechnology, California, USA). Anti-mouse, anti-rabbit and anti-goat IgG HRP-linked antibodies were purchased from GE Healthcare (Amersham, UK). Human apoA-I was purchased from Sigma-Aldrich. Human acetylated LDL (acLDL) and human HDL-C were purchased from Biomedical Technologies, Inc. (Stoughton, MA, USA). [1, 2-^{3}H (N)]-Cholesterol was purchased from Perkin Elmer (Boston, MA, USA). T0901317 was purchased from Cayman Chemical (Ann Arbor, MI, USA).

Generation of miR-33b KI mice. A targeting vector was constructed by modifying bacterial artificial chromosome RP24-310C22 (Invitrogen) using a defective prophage λ-Red recombination system[25,26]. As a selection marker, a neomycin resistance cassette flanked by loxP sites (loxP-PGK-gb2-neo-loxP cassette; Gene Bridges, Germany) was inserted at the adjacent site of the human pre-miR-33b site. The targeting vector was electroporated into C57BL/6 mouse ES cells (DS Pharma Biomedical) using a Nucleofector system (Lonza). Positive clones were selected by incubating cells with 200 μg/ml geneticin (Invitrogen) for 5 days, and homologous recombination was confirmed by Southern blotting. Successfully recombined ES cells were injected into blastocysts from ICR strain mice supplied by Unitech Inc. (Japan), and chimeric mice were bred with C57BL/6 mice to generate F1 mice. F1 mice genotypes were confirmed by Southern blotting. The neomycin resistance cassette was removed from the mouse germ line by breeding heterozygous mice with *Ayu-1 Cre* KI mice, which expressed Cre recombinase in multiple tissues, including the germ line[27]. Descendant miR-33b knock-in heterozygous mice without the *Ayu-1 Cre* allele were crossed with each other to generate the miR-33b KI$^{+/+}$ mice. All experiments were performed with male C57BL/6 background mice and wild-type littermates were used as a control. All of the experimental protocols were approved by the Ethics Committee for Animal Experiments of Kyoto University and the methods were performed in *accordance* with the guidelines approved by the ethics committee. Primers used for genotyping were as follows: WT/KI sense, ATGGATTTACC-TCAGTTTTAACGAC; WT antisense, CATCACTGAAGCACTGCATCTGC; KI antisense, AAGTGGATCCAGAATTCGTGA; *Cre* sense, GCTGCCACGACdC-AAGTGACAGCAATG; and *Cre* antisense, GTAGTTATTCGGATCATCAGC-TACAC.

Southern blotting. Southern blotting was performed using DIG High Prime DNA Labeling and Detection Starter Kit II (Roche) according to the manufacturer's protocol. Genomic DNA samples were purified and digested with MfeI and AseI for a 5′ probe, EcoRI for a 3′ probe, and NheI for a Neo probe. Primer sequences used to amplify these probes were as follows:

5′ probe sense, CACGGTTGTGAGAAGTCAGTATTC; 5′ probe antisense, CTTTGCAAGCTCCTTGAGAATAAG; 3′ probe sense, AGTAAAATTCTCCTC-AATGAACGTG; 3′ probe antisense, CAGTAGGTGACATTGTGATTGATCT; Neo probe sense, GAACAAGATGGATTGCACGCAGGTTCTCCG; and Neo probe antisense, GTAGCCAACGCTATGTCCTGATAG.

Determination of splicing between exons 16 and 17 in *Srebf1*. We amplified the fragment between *Srebf1* exons 13 and 17 using cDNA from the livers of the indicated mice by PCR, and these products were then electrophoresed. Extension time was sufficient to expand the fragment when the correct splicing did not occur. There was no other band except for that of the correct size. Sequencing was performed using a primer for exon 16 and an ABI 3130 genetic analyzer. Primer sequences used were as folows:

Exon 13 sense, CCTAGAGCGAGCGTTGAACT; Exon 17 antisense, CTACCT-GGACTGAAGCTGGTG; and Exon 16 sequence primer, AGGGCAGCTCTGTAC-TCCTTC.

Cell culture. HepG2 cells were cultured in Dulbecco's modified Eagle's medium (DMEM; Nacalai Tesque, Japan) supplemented with 10% fetal bovine serum (FBS). Mouse primary hepatocytes were obtained from miR-33b KI$^{+/+}$ mice using a two-step collagenase perfusion method[28]. In brief, hepatocyte suspensions were obtained by passing a collagenase type II (Gibco BRL, Life Technologies Inc., Rockville, MD, USA)-digested liver sample through a 70-μm cell strainer, followed by centrifugation to isolate mature hepatocytes. Hepatocytes were then resuspended in DMEM supplemented with 10% FBS and seeded on collagen type I-coated dishes (Iwaki Asahi Glass Co. Ltd., Japan) at a density of 7×10^4 cells/ml. After incubation for 24 h, the cells were used for experiments.

Cholesterol efflux from macrophages. Cellular cholesterol efflux via apoA-I was determined as described previously[29]. In brief, thioglycollate-elicited mouse peritoneal macrophages were plated in 24-well microplates at a density of 5×10^6 cells/ml. Cells were cultured for 24 h in RPMI 1640 containing ^{3}H-labeled acLDL (1.0 μCi/ml of ^{3}H-cholesterol and 25 μg/ml of acLDL). On the next day, the cells were washed 3 times with RPMI 1640 and incubated for 6 h in RPMI 1640 with or without apoA-I (10 μg/ml) or HDL (100 μg/ml). Cholesterol efflux was expressed as the percentage of radioactivity released from cells in medium relative to the total radioactivity in cells plus medium.

Western blotting. Western blotting was performed using standard procedures as described previously[30]. A lysis buffer was supplemented with a complete mini protease inhibitor (Roche), ALLN (25 μg/ml), 0.5 mM NaF, and 10 μM Na_3VO_4 just prior to use. Protein concentrations were determined using a bicinchoninic acid protein assay kit (Bio-Rad). All samples (20 μg of protein) were suspended in lysis buffer, fractionated using NuPAGE 4%–12% Bis-Tris (Invitrogen) gels, and transferred to a Protran nitrocellulose transfer membrane (Whatman). The membrane was blocked using 1× phosphate-buffered saline (PBS) containing 5% non-fat milk for 1 h and incubated with a primary antibody [anti-ABCA1 (1 : 1000), anti-ABCG1 (1 : 1000), anti-AMPKα (1 : 1000), anti-SREBP-1 (1 : 250), anti-TF2B (1 : 1000), anti-β-actin (1 : 3000), anti-CREB (1 : 1000), anti-PCK1 (1 : 1000), anti-SRC1 (1 : 200), anti-G6Pase (1 : 200) or anti-CPT1a (1 : 1000)] overnight at 4°C. After washing with PBS–0.05% Tween 20 (0.05% T-PBS), the membrane was incubated with a secondary antibody (anti-rabbit, anti-mouse and anti-goat IgG HRP-linked; 1 : 2000) for 1 h at 4°C. The membrane was then washed with 0.05% T-PBS and detected with an ECL Western Blotting Detection Reagent (GE Healthcare) using an LAS-1000 system (Fuji Film).

RNA extraction and quantitative RT-PCR (qRT-PCR). Total RNA was isolated and purified using TriPure Isolation Reagent (Roche). cDNA was synthesized from 1 μg of total RNA using the Transcriptor First Strand cDNA Synthesis Kit (Roche) according to the manufacturer's instructions. For qRT-PCR, specific genes were amplified in 40 cycles using SYBR™ Green PCR Master Mix (Applied Biosystems). Expression was normalized to that of the housekeeping gene β-actin. Gene-specific primers are as follows;

SREBF1 sense, AACAGTCCCACTGGTCGTAGAT; *SREBF1* antisense, TGTTGCAGAAAGCGAATGTAGT; *SREBF2* sense, AGGAGAACATGGTG-CTGA; *SREBF2* antisense, TAAAGGAGAGGCACAGGA; *ACTB* sense, AGGCA-CTCTTCCAGCCTTCC; *ACTB* antisense, GCACTGTGTTGGCGTACAGG; *Srebf1* sense, TAGAGCATATCCCCCAGGTG; *Srebf1* antisense, GGTACGGGCCAC-AAGAAGTA; *Srebf2* sense, GTGGAGCAGTCTCAACGTCA; *Srebf2* antisense, TGGTAGGTCTCACCCAGGAG; *Actb* sense, GATCTGGCACCACACCTTCT; and *Actb* antisense, GGGGTGTTGAAGGTCTCAAA.

Quantitative PCR for miRs. Total RNA was isolated using the TriPure Isolation Reagent (Roche). miR-33a and miR-33b were measured using TaqMan MicroRNA assay protocols (Applied Biosystems). Products were analyzed using a thermal cycler (ABI Prism® 7900HT sequence detection system). miRs expression of samples were normalized by U6 snRNA expression.

Serum biochemical analysis. After mice were fasted for 4–6 h, blood was obtained from the inferior vena cava of an anesthetized mouse, and serum was separated by centrifugation at 4°C and stored at −80°C. Employing standard methods, biochemical measurements were made using a Hitachi 7180 Auto Analyzer (Nagahama Life Science Laboratory, Nagahama, Japan). Lipoproteins were analyzed by HPLC at Skylight Biotech (Akita, Japan), according to the procedures described previously[31].

Statistical analysis. Results are given as mean ± s.e.m. Statistical comparisons were made using unpaired two-tailed Student's *t*-tests or one-way analysis of variance with the Bonferroni post hoc test, as appropriate. A p value of <0.05 was considered significant.

1. Osborne, T. F. & Espenshade, P. J. Evolutionary conservation and adaptation in the mechanism that regulates SREBP action: what a long, strange tRIP it's been. *Genes Dev* **23**, 2578–2591 (2009).

2. Espenshade, P. J. & Hughes, A. L. Regulation of sterol synthesis in eukaryotes. *Annu Rev Genet* **41**, 401–427 (2007).
3. Horton, J. D., Goldstein, J. L. & Brown, M. S. SREBPs: activators of the complete program of cholesterol and fatty acid synthesis in the liver. *J Clin Invest* **109**, 1125–1131 (2002).
4. Yokoyama, C. *et al.* SREBP-1, a basic-helix-loop-helix-leucine zipper protein that controls transcription of the low density lipoprotein receptor gene. *Cell* **75**, 187–197 (1993).
5. Ono, K., Kuwabara, Y. & Han, J. MicroRNAs and Cardiovascular Diseases. *FEBS J* (2011).
6. Najafi-Shoushtari, S. H. *et al.* MicroRNA-33 and the SREBP host genes cooperate to control cholesterol homeostasis. *Science* **328**, 1566–1569 (2010).
7. Rayner, K. J. *et al.* MiR-33 contributes to the regulation of cholesterol homeostasis. *Science* **328**, 1570–1573 (2010).
8. Horie, T. *et al.* MicroRNA-33 encoded by an intron of sterol regulatory element-binding protein 2 (Srebp2) regulates HDL in vivo. *Proc Natl Acad Sci U S A* **107**, 17321–17326 (2010).
9. Rayner, K. J. *et al.* Antagonism of miR-33 in mice promotes reverse cholesterol transport and regression of atherosclerosis. *J Clin Invest* **121**, 2921–2931 (2011).
10. Horie, T. *et al.* MicroRNA-33 Deficiency Reduces the Progression of Atherosclerotic Plaque in ApoE(−/−) Mice. *J Am Heart Assoc* **1**, e003376 (2012).
11. Horie, T. *et al.* MicroRNAs and Lipoprotein Metabolism. *J Atheroscler Thromb* **21**, 17–22 (2014).
12. Sowa, N. *et al.* MicroRNA 26b encoded by the intron of small CTD phosphatase (SCP) 1 has an antagonistic effect on its host gene. *J Cell Biochem* **113**, 3455–3465 (2012).
13. DeBose-Boyd, R. A., Ou, J., Goldstein, J. L. & Brown, M. S. Expression of sterol regulatory element-binding protein 1c (SREBP-1c) mRNA in rat hepatoma cells requires endogenous LXR ligands. *Proc Natl Acad Sci U S A* **98**, 1477–1482 (2001).
14. Ramirez, C. M. *et al.* MicroRNA 33 regulates glucose metabolism. *Mol Cell Biol* **33**, 2891–2902 (2013).
15. Basso, F. *et al.* Role of the hepatic ABCA1 transporter in modulating intrahepatic cholesterol and plasma HDL cholesterol concentrations. *J Lipid Res* **44**, 296–302 (2003).
16. Timmins, J. M. *et al.* Targeted inactivation of hepatic Abca1 causes profound hypoalphalipoproteinemia and kidney hypercatabolism of apoA-I. *J Clin Invest* **115**, 1333–1342 (2005).
17. Shimano, H. SREBPs: physiology and pathophysiology of the SREBP family. *FEBS J* **276**, 616–621 (2009).
18. Horie, T. *et al.* MicroRNA-33 regulates sterol regulatory element-binding protein 1 expression in mice. *Nat Commun* **4**, 2883 (2013).
19. Gerin, I. *et al.* Expression of miR-33 from an SREBP2 intron inhibits cholesterol export and fatty acid oxidation. *J Biol Chem* **285**, 33652–33661 (2010).
20. Fernandez-Hernando, C. & Moore, K. J. MicroRNA modulation of cholesterol homeostasis. *Arterioscler Thromb Vasc Biol* **31**, 2378–2382 (2011).
21. Rayner, K. J. *et al.* Inhibition of miR-33a/b in non-human primates raises plasma HDL and lowers VLDL triglycerides. *Nature* **478**, 404–407 (2011).
22. Zhou, X. *et al.* Genetic deletion of low density lipoprotein receptor impairs sterol-induced mouse macrophage ABCA1 expression. A new SREBP1-dependent mechanism. *J Biol Chem* **283**, 2129–2138 (2008).
23. Memczak, S. *et al.* Circular RNAs are a large class of animal RNAs with regulatory potency. *Nature* **495**, 333–338 (2013).
24. Rottiers, V. *et al.* Pharmacological Inhibition of a MicroRNA Family in Nonhuman Primates by a Seed-Targeting 8-Mer AntimiR. *Sci Transl Med* **5**, 212ra162 (2013).
25. Copeland, N. G., Jenkins, N. A. & Court, D. L. Recombineering: a powerful new tool for mouse functional genomics. *Nat Rev Genet* **2**, 769–779 (2001).
26. Horiguchi, M. *et al.* Fibulin-4 conducts proper elastogenesis via interaction with cross-linking enzyme lysyl oxidase. *Proc Natl Acad Sci U S A* **106**, 19029–19034 (2009).
27. Morita, M. *et al.* HLF/HIF-2alpha is a key factor in retinopathy of prematurity in association with erythropoietin. *EMBO J* **22**, 1134–1146 (2003).
28. Seglen, P. O. Preparation of isolated rat liver cells. *Methods Cell Biol* **13**, 29–83 (1976).
29. Zhang, Z. *et al.* Expression of cholesteryl ester transfer protein in human atherosclerotic lesions and its implication in reverse cholesterol transport. *Atherosclerosis* **159**, 67–75 (2001).
30. Horie, T. *et al.* Acute doxorubicin cardiotoxicity is associated with miR-146a-induced inhibition of the neuregulin-ErbB pathway. *Cardiovasc Res* **87**, 656–664 (2010).
31. Usui, S., Kakuuchi, H., Okamoto, M., Mizukami, Y. & Okazaki, M. Differential reactivity of two homogeneous LDL-cholesterol methods to LDL and VLDL subfractions, as demonstrated by ultracentrifugation and HPLC. *Clin Chem* **48**, 1946–1954 (2002).

Acknowledgments

We thank Neal G. Copeland (Institute of Molecular and Cell Biology, Singapore) for the defective prophage λ-Red recombination system; Junji Takeda (Osaka University, Osaka, Japan) and Kosuke Yusa (Osaka University, Osaka, Japan) for the plasmid used for the construction of the targeting vector; Ken-ichi Yamamura (Kumamoto University, Kumamoto, Japan) and Kimi Araki (Kumamoto University) for *Ayu-1* Cre expressing mice. This work was supported in part by grants from the Japan Society for the Promotion of Science, by a Grant-in-Aid for Scientific Research from the Ministry of Education, Culture, Sports, Science, and Technology of Japan (to T. Kimura, T. Kita, K.H., T.H., and K.O.), by a Grant-in-Aid for Scientific Research on Innovative Areas "Crosstalk between transcriptional control and energy pathways, mediated by hub metabolites"(3307) from the Ministry of Education, Culture, Sports, Science and Technology of Japan (to K.O.), by Otsuka Pharmaceutical Co., Ltd. - Kyoto University SRP Program (to T. Kimura, T. Kita, M.Y., T.H., and K.O.), by grants from Banyu Life Science Foundation International, Takeda Memorial Foundation, Suzuken Memorial Foundation, Sakakibara Memorial Foundation, Japan Foundation of Applied Enzymology, SENSHIN Medical Research Foundation, Kowa Life Science Foundation, and ONO Medical Research Foundation (to T.H.), and by grants from ONO Medical Research Foundation, the Cell Science Research Foundation, Daiichi-Sankyo Foundation of Life Science, and Takeda Memorial Foundation (to K.O.).

Author contributions

T.H., T.N. and K.O. designed the project; T.H., T.N., O.B., Y.K., T.N., M.N., S.U., M.I., F.N., Y.I., S.K. and N.S. performed experiments; T.H., T.N., N.Y., H.S., T.N., K.H., N.K., M.Y., T.K., T.K. and K.O. analyzed and interpreted data; and T.H., T.N. and K.O. prepared the manuscript.

Additional information

Supplementary information accompanies this paper at http://www.nature.com/scientificreports

Competing financial interests: The authors declare no competing financial interests.

How to cite this article: Horie, T. *et al.* MicroRNA-33b knock-in mice for an intron of sterol regulatory element-binding factor 1 (*Srebf1*) exhibit reduced HDL-C *in vivo*. *Sci. Rep.* **4**, 5312; DOI:10.1038/srep05312 (2014).

Genes to Cells

Deacetylation of phosphoglycerate mutase in its distinct central region by SIRT2 down-regulates its enzymatic activity

Takeshi Tsusaka[1], Tingting Guo[1], Teiti Yagura[1], Toshiaki Inoue[2], Masayuki Yokode[3], Nobuya Inagaki[1] and Hiroshi Kondoh[1,4]*

[1]*Department of Diabetes, Endocrinology and Nutrition, Graduate School of Medicine, Kyoto University, 54 Kawahara-cho, Shogoin, Sakyo-ku, Kyoto 606-8507, Japan*
[2]*Division of Human Genome Science, Department of Molecular and Cellular Biology, School of Life Sciences, Faculty of Medicine, Tottori University, 86 Nishi-cho, Yonago, Tottori 683-8503, Japan*
[3]*Department of Clinical Innovative Medicine, Translational Research Center, Kyoto University Hospital, 54 Kawahara-cho, Shogoin, Sakyo-ku, Kyoto 606-8507, Japan*
[4]*Geriatric Unit, Graduate School of Medicine, Kyoto University, 54 Kawahara-cho, Shogoin, Sakyo-ku, Kyoto 606-8507, Japan*

Substantially high rate of glycolysis, known as the Warburg effect, is a well-known feature of cancers, and emerging evidence suggests that it supports cancerous proliferation/tumor growth. Phosphoglycerate mutase (PGAM), a glycolytic enzyme, is commonly up-regulated in several cancers, and recent reports show its involvement in the Warburg effect. Here, a comprehensive analysis shows that PGAM is acetylated at lysines 100/106/113/138 in its central region, and a member of the Sirtuin family (class III deacetylase), SIRT2, is responsible for its deacetylation. Over-expression of SIRT2 or mutations at the acetylatable lysines of PGAM attenuates cancer cell proliferation with a concomitant decrease in PGAM activity. We also report that the acetyltransferase PCAF (p300/CBP-associated factor) interacts with PGAM and acetylates its C-terminus, but not the central region. As prior evidence suggests that SIRT2 functions as a tumor suppressor, our results would provide support for the mechanistic basis of this activity.

Introduction

Several properties of cancer cells, such as immortalization, evasion from apoptotic stimuli, transformation, anchorage-independent growth, metastasis, and invasiveness, make them distinguishable from their normal counterparts and could be possible targets for anticancer therapy. Protein levels and activities of many glycolytic enzymes are frequently up-regulated in cancerous cells, *in vitro* and *in vivo*. This enhanced glycolysis is also a well-known property of many cancerous cells and is known as the Warburg effect (Warburg 1956). As glycolysis is vital for energy production in normal cells and tissues too, it is necessary to understand the Warburg effect and how it is coupled with other hallmarks of cancer to specifically target it in a potential anticancer therapy.

Communicated by: Takashi Toda
**Correspondence:* hkondoh@kuhp.kyoto-u.ac.jp

Phosphoglycerate mutase (PGAM), is a glycolytic enzyme, which catalyzes the conversion of 3-phosphoglycerate (3-PG) into 2-phosphoglycerate (2-PG). Among all glycolytic enzymes, the impacts of PGAM on cancer growth and the Warburg effect have been reported by several groups. First, PGAM activity is up-regulated in many types of cancer (Durany *et al.* 1997; Ren *et al.* 2010). Additionally, an inhibitor of PGAM, MJE3, was isolated as the most potent anticancer compound against breast cancer cells (Evans *et al.* 2005). PGAM knockdown retards cancerous proliferation (Ren *et al.* 2010; Hitosugi *et al.* 2012) and provokes premature senescence in primary cells (Kondoh *et al.* 2005). The cancer-specific isoform pyruvate kinase M2 (PKM2) activates an alternative glycolytic pathway, accompanied by enhancement of

DOI: 10.1111/gtc.12176

PGAM activity (Vander Heiden *et al.* 2010). Finally, PGAM is implicated in an experimental neoplastic transformation process (Mikawa *et al.* 2014). Collectively, the significance of PGAM on the Warburg effect has been well established, although, until recently, it was not clear how PGAM is dysregulated in cancer.

Interestingly, although glycolytic enhancement in cancer is partly mediated by transcriptional regulation, via hypoxia inducible factor-1 (HIF-1; Iyer *et al.* 1998), PGAM is an exception, not being subject to regulation by HIF-1. In contrast, post-translational regulation of PGAM is more important than transcriptional control for modulating PGAM activity. PGAM is phosphorylated by Pak1 or ubiquitinated by p53/Mdm2 axis to down-regulate its activity under senescence-inducing stresses (Shalom-Barak & Knaus 2002; Mikawa *et al.* 2014), whereas PGAM is phosphorylated by tyrosine kinases to up-regulate its activity in cancer cells (Hitosugi *et al.* 2013).

Acetylation is known to be crucial for post-translational regulation of many proteins, including glycolytic and many other metabolic enzymes, whose dysregulation may contribute to cancerous metabolism (Zhao *et al.* 2010; Lin *et al.* 2013). Consistently, it has been shown that Sirtuins, which are NAD^+-dependent deacetylases, have pivotal roles in cancer and its metabolism. In mammals, there are seven family members (SIRT1–7) that share a consensus domain, which catalyzes mono-ribosyltransfer, deacetylation, or deacylation. Some SIRT knockout mice (SIRT2, SIRT3, SIRT4, and SIRT6) displayed cancer-prone phenotypes (Kim *et al.* 2010, 2011; Sebastian *et al.* 2012; Jeong *et al.* 2013; Serrano *et al.* 2013), suggesting that these Sirtuins might function as tumor suppressors.

Here, we report that SIRT2 interacts with PGAM, resulting in its deacetylation. Deacetylation of PGAM in its central region by SIRT2 down-regulates its activity and attenuates proliferation in HCT116 cancer cells, implicating that the acetylation of PGAM is closely coupled with cancerous proliferation.

Results

Acetylation status and enzymatic activity of PGAM are different in cancer cell lines

Among several human colon cancer cell lines, including HCT116, DLD-1, SW480, SW620, SW48, and RKO, we examined the acetylation of PGAM1 and PGAM2, which are highly homologous (78.7% identity in human, 80.7% in mouse). The acetylation levels of introduced 3xFLAG-tagged PGAM1 or PGAM2 were assessed using an anti-acetylated lysine antibody (AcK) as a probe after immunoprecipitation using anti-FLAG antibodies. As shown in Fig. 1A, it was observed that the acetylation levels for PGAM1 were quite different among the cell lines, and HCT116 cells displayed the highest acetylation levels. We also observed that treatment with deacetylase inhibitors (D.I.), including tricostatin A (TSA) and nicotinamide (NAM), did not affect the acetylation levels for PGAM in these cells, suggesting that PGAM was not continuously deacetylated in our experimental conditions. In the case of PGAM2, a similar result was obtained (Fig. 1B). Next, comparative analyses for protein level and enzymatic activity were carried out. Although it was observed that PGAM protein levels were rather constant (Fig. 1C), PGAM enzymatic activities were very different (Fig. 1D). HCT116 cells exhibited the highest PGAM activity among the cell lines used in this study. Collectively, these data indicate the possibility that the acetylation status in HCT116 cells is closely correlated with high PGAM activity.

Identification of the acetylated residues of PGAM in HCT116 cells

Next, the positions of acetylated residues of PGAM in HCT116 cells were explored. Proteomic approaches have previously disclosed that lysines 5 (only in PGAM1), 61, 100, 106, 113, and 225 of PGAM are acetylated (Kim *et al.* 2006; Choudhary *et al.* 2009; Hebert *et al.* 2013), whereas lysines 251, 253, and 254 in the carboxy-terminus of PGAM1 have been identified in HEK293 cells by a mutagenesis approach (Hallows *et al.* 2012). To identify acetylated residues of PGAM in HCT116 cells with no bias, we applied a site-directed mutagenesis approach against all lysine residues in PGAM. The twenty lysines in PGAM2 were separated into four groups; five lysines in the N-terminus, seven lysines in the central region, five lysines as a third group, and three lysines in the C-terminus. We generated mutants with substitutions of lysines by arginines in each of these groups, designated as Nter 5KR, 7KR, Mid 5KR, and Cter3KR, respectively (Fig. 2A, upper panel). A PGAM mutant with the substitutions of all twenty lysines into arginines (referred to as All KR) was also generated as a nonacetylatable control. In HCT116 cells, the acetylation levels between wild-type and

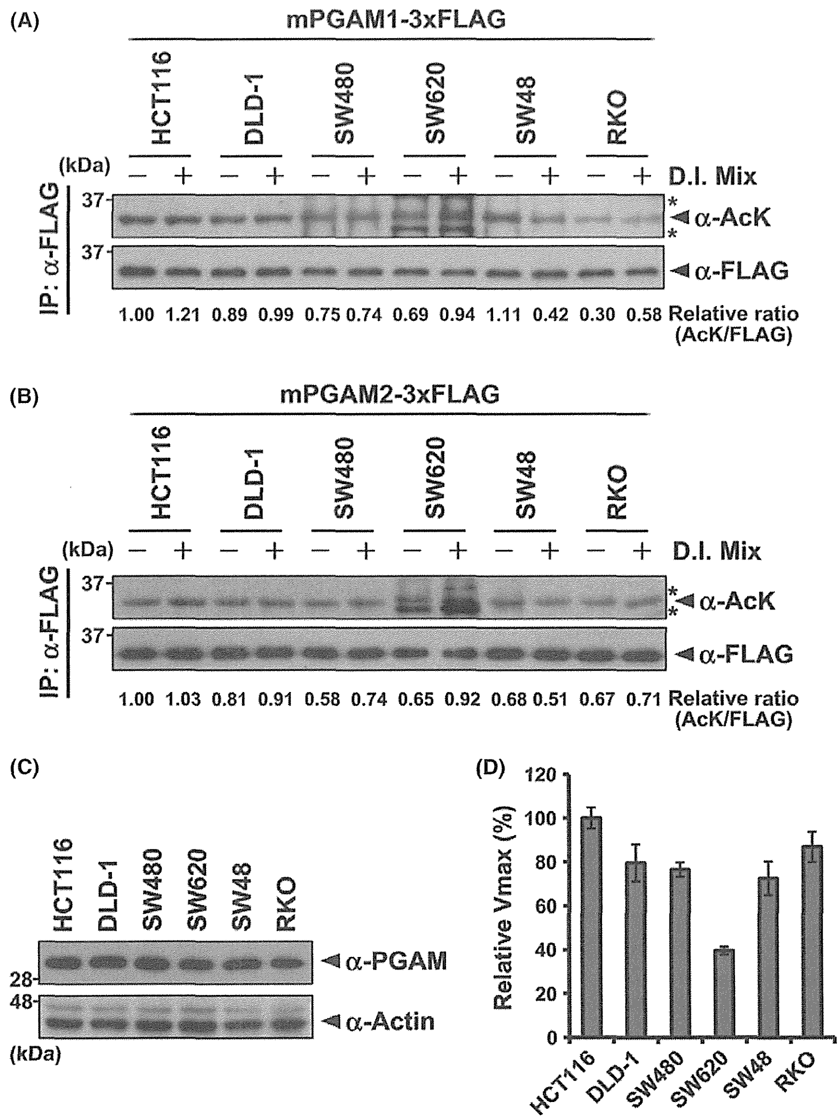

Figure 1 Comparison of PGAM enzymatic activity and acetylation levels in cancer cell lines. (A, B) 3xFLAG-tagged PGAM1 (A) or PGAM2 (B) was transiently expressed in the cancer cell lines. The cells were treated with or without 5 mM NAM and 5 μM TSA for 12 h. The PGAM acetylation levels were assessed using anti-pan acetylated lysine (AcK) or FLAG antibodies as probes after immunoprecipitation (IP) with FLAG M2 affinity gel. Asterisks indicate non-specific bands. (C, D). The total cell extracts were subjected to Western blot analysis with the indicated antibodies (C) and measurement of PGAM activity (D). Error bars represent SEM (n = 3).

these PGAM mutants were compared. As shown in Fig. 2B, the acetylation levels of the 7KR mutant were identical to those in the All KR mutant, suggesting that the acetylation of PGAM in HCT116 cells was located in the central region, having seven lysines (K100, K106, K113, K129, K138, K146, and K157). To specify the acetylated residues in this central region, first, the seven lysines were separated into two parts, lysines 100/106/113/129 and lysines 138/146/157. The lysines were substituted to arginines (referred to as K100/106/113/129R and K138/146/157R, respectively), and their acetylation levels were assessed in HCT116 cells. Both K100/106/113/129R and K138/146/157R mutants showed lower acetylation levels when compared to wild-type (Fig. S1A in Supporting Information), but distinct from those observed in the 7KR mutant. As shown in Fig. S1B and C (left panels) in Supporting Information, we

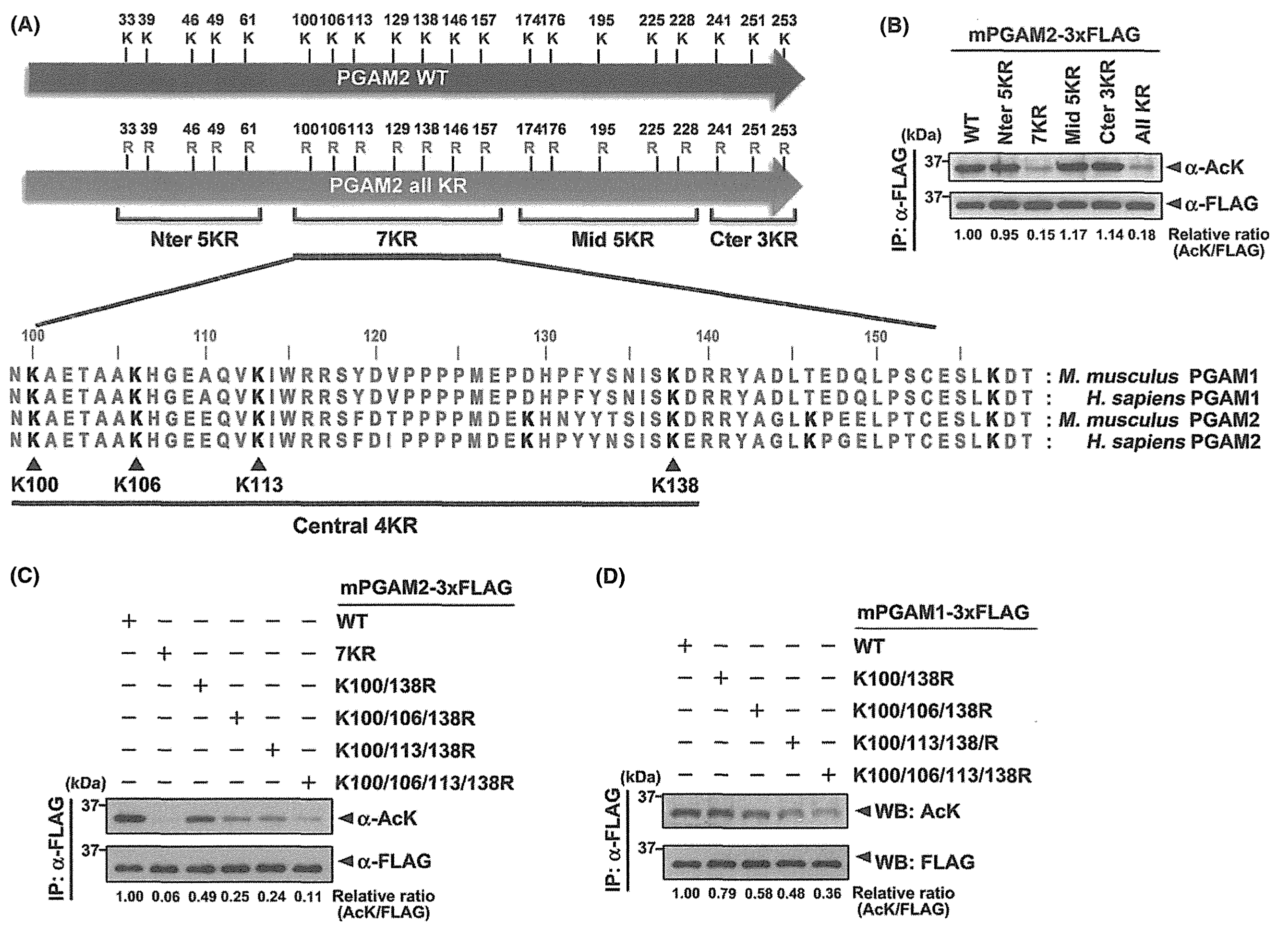

Figure 2 Identification of acetylated residues of PGAM in HCT116 cells. (A). Schematic diagrams of wild-type (WT) and lysine mutants (KR) of PGAM2 (top panel). Alignment of amino acid sequences of PGAM1 and PGAM2 from different species. Lysine residues are indicated in black. Identified acetylated lysine residues are indicated by arrow heads (lower panel). (B, C, D) Each of the lysine residues of PGAM2 (B) or some of them in PGAM2 (C) or PGAM1 (D) were mutated to arginine, and these mutants were transiently expressed in HCT116 cells. The acetylation of mutants was assessed using antipan acetylated lysine (AcK) or FLAG antibodies as probes after immunoprecipitation (IP) with FLAG M2 affinity gel.

introduced an additional substitution in each mutant. We found that mutants with such additional substitution at lysine 100, 106, 113, or 138 displayed a decrease in PGAM acetylation (Fig. S1B and C, right panels in Supporting Information). Finally, it was observed that K100/106/113/138R mutations almost abolished the acetylation of PGAM2, mostly like the 7KR mutant (Fig. 2C). This suggests that PGAM2 is mainly acetylated at lysines 100/106/113/138, which are highly conserved between PGAM1 and PGAM2 in humans and mice. We further validated that K100/106/113/138R mutations in PGAM1 almost abolished its acetylation (Fig. 2D). Together, these results indicate that lysines 100/106/113/138 are the main acetylated residues of both PGAM1 and PGAM2 in HCT116 cells (Fig. 2A, lower panel).

Sirtuins, including SIRT1, SIRT2, SIRT3, SIRT4, and SIRT6, interact with PGAM

It has been reported that SIRT1 is the deacetylase for the C-terminus of PGAM1 in HEK293 cells (Hallows *et al.* 2012), whereas it was observed that the central region of both PGAM1 and PGAM2 is mainly acetylated in HCT116 cells. Therefore, we first examined the interaction between the seven Sirtuins and PGAM in HCT116 cells. HCT116 cells were separately co-transfected with each member of Sirtuins (V5-tagged), together with 3xFLAG-tagged

PGAM1, and the cell extracts were subjected to immunoprecipitation. Surprisingly, we found that PGAM1 interacts not only with SIRT1, but also with other Sirtuins, including SIRT2, SIRT3, SIRT4, and SIRT6 (Fig. 3A, B). It is noteworthy that SIRT2 interacts most strongly with PGAM1 in HCT116 cells, whereas SIRT1 does so modestly. We next examined whether lysine-to-arginine (KR) mutations in the central regions diminish the interaction between PGAM1 and SIRT2. As shown in Fig. 3C, the interaction between PGAM1 and SIRT2 was not affected by KR mutations. In the case of PGAM2, a similar result was obtained (Fig. 3D).

Ectopic expression of SIRT2 decreases the acetylation levels of PGAM

These findings suggest the possibility that not only SIRT1, but also SIRT2 could deacetylate PGAM. HCT116 cells were infected with retroviruses encoding wild-type (WT) SIRT2, a catalytically inactive mutant (HY) SIRT2, or vector control, and were subsequently selected by puromycin treatment. These stably infected cells were transfected with PGAM1 (Fig. 4A) or PGAM2 (Fig. 4B), followed by the examination of the acetylation status. As shown in Fig. 4A, B, the acetylation levels of both PGAM1 and PGAM2 in SIRT2-WT-expressing cells were lower when compared to those in control and SIRT2-HY-expressing cells, suggesting that the catalytic activity of SIRT2 is required for deacetylation of PGAM. Importantly, in sharp contrast to SIRT2, SIRT1-expressing HCT116 cells exhibited acetylation levels of PGAM similar to those in control (Fig. 4C). These results suggest that SIRT2, but not SIRT1, is responsible for PGAM deacetylation in HCT116 cells.

Ectopic expression of SIRT2 decreases the enzymatic activity of PGAM and inhibits cell proliferation

To explore the functional role of SIRT2-dependent deacetylation of PGAM, PGAM enzymatic activity was measured in SIRT2-WT, SIRT2-HY, and

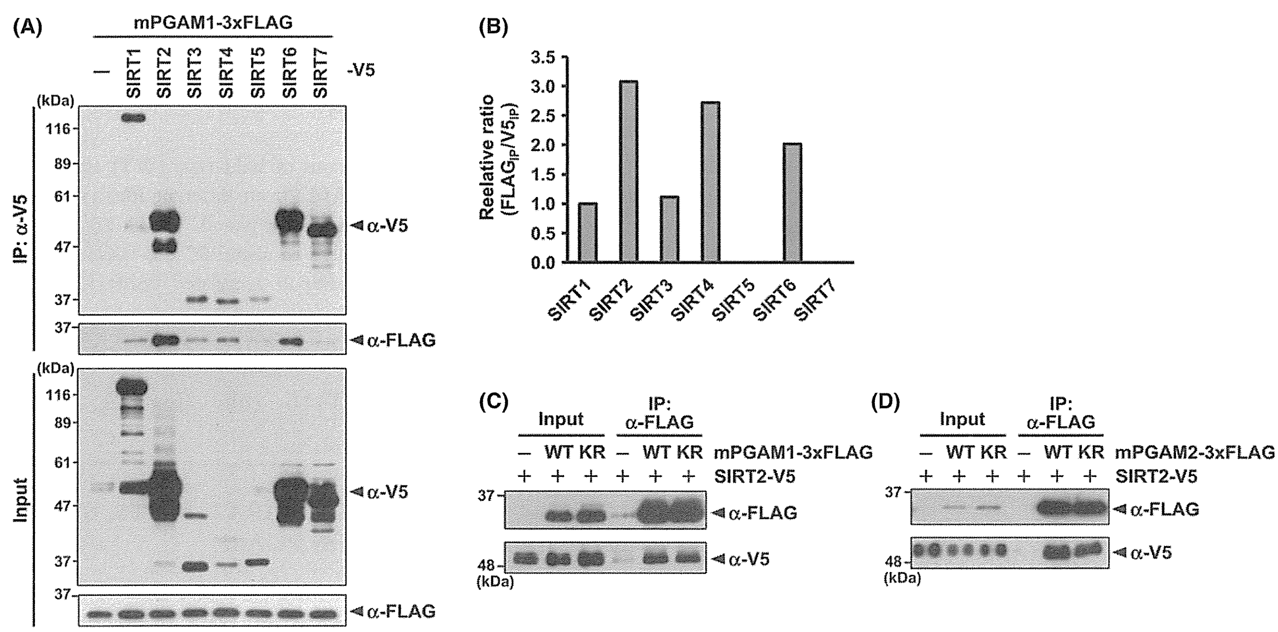

Figure 3 Physical interaction of PGAM with a cytoplasmic deacetylase, SIRT2. (A, B). Each V5-tagged Sirtuin or an empty vector was individually co-transfected with 3xFLAG-tagged PGAM1. The cell extracts were subjected to immunoprecipitation (IP) with V5-conjugated beads followed by Western blot analysis with the indicated antibodies (A). Ratios of anti-FLAG bands relative to anti-V5 bands were calculated through densitometric analysis of the IP sample (B). (C, D SIRT2 was individually co-transfected with WT PGAM1, KR-mutant PGAM1, or empty vector (all 3xFLAG-tagged) in HCT116 cells. The cell extracts were subjected to immunoprecipitation (IP) with FLAG M2 affinity gel followed by Western blot analysis with the indicated antibodies (C). Similar results were obtained for PGAM2 (D).

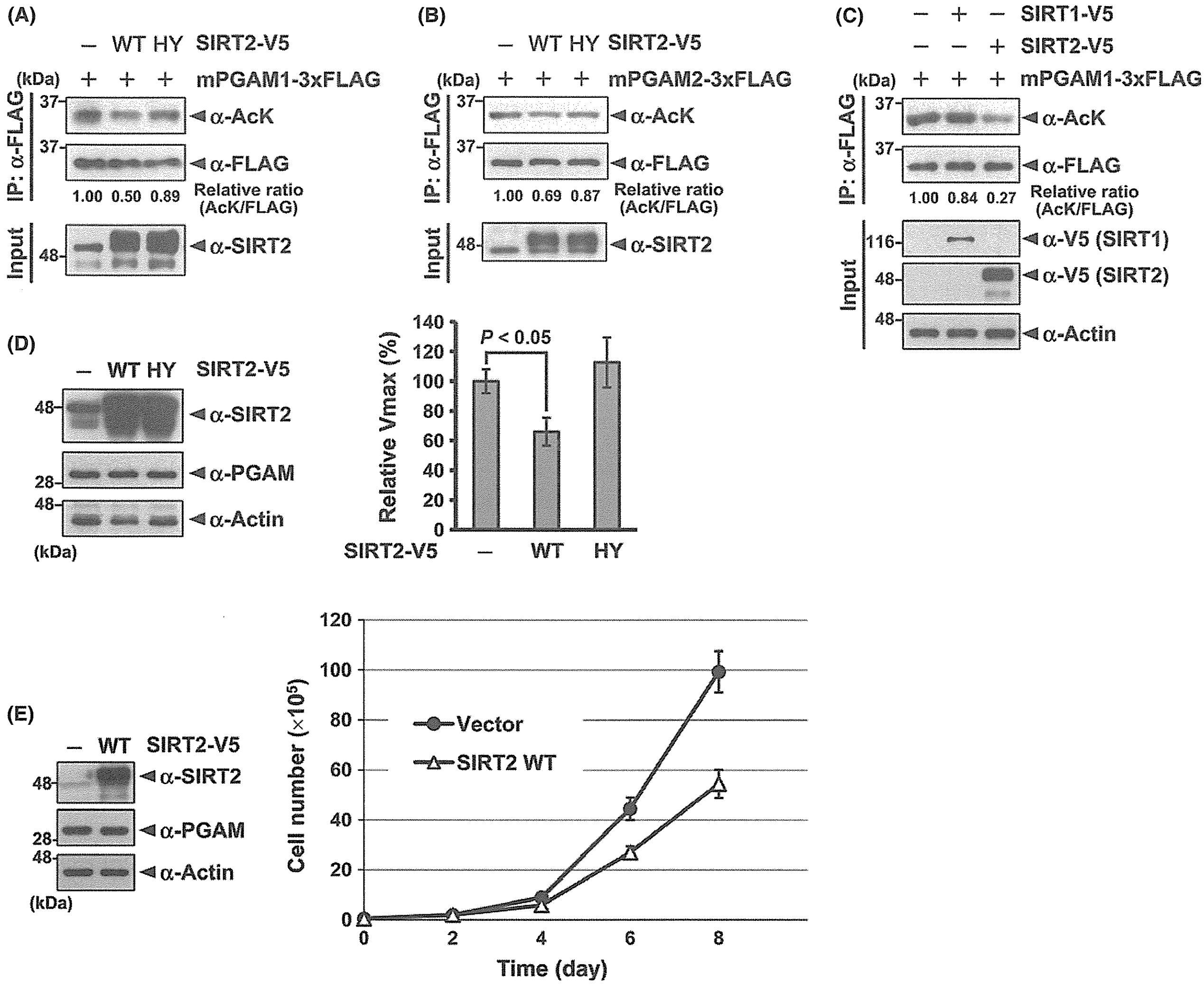

Figure 4 Down-regulation of PGAM activity by SIRT2 via its deacetylation. (A, B) HCT116 cells were stably transfected with either control vector, wild-type (WT) SIRT2-, or catalytically inactive mutant (HY) SIRT2-over-expression vector. 3xFLAG-tagged PGAM1 (A) or PGAM2 (B) was transiently expressed in the stably transfected cells. The PGAM acetylation levels were assessed using antipan acetylated lysine (AcK) or FLAG antibodies as probes after immunoprecipitation (IP) with FLAG M2 affinity gel. (C) HCT116 cells were stably transfected with either control vector, SIRT1-, or SIRT2-over-expression vector. 3xFLAG-tagged wild-type PGAM1 was transiently expressed in the stably transfected cells. The PGAM acetylation levels were assessed using antipan acetylated lysine (AcK) or FLAG antibodies as probes after immunoprecipitation (IP) with FLAG M2 affinity gel. (D) HCT116 cells were stably transfected with either control vector, SIRT1-, or SIRT2-over-expression vector. The total cell extracts were subjected to Western blot analysis with the indicated antibodies (left panel) and measurement of PGAM activity (right panel). Error bars represent SEM (n = 4). Statistical analysis was carried out using a *t-test*. (E) SIRT2-expressing HCT116 stable cell lines were generated (left panel). An equal number of the stably transfected cells were seeded in a 6-well plate. Cell numbers were counted every 48 h. Error bars represent SD.

control cells. Western blot analysis showed that the ectopic expression of SIRT2-WT or SIRT2-HY did not affect endogenous PGAM protein levels (Fig. 4D, left panel). However, PGAM activity in SIRT2-WT-expressing cells was approximately 40% lower than that in vector control or SIRT2-HY-expressing cells (Fig. 4D, right panel). Previously, several groups reported that inhibition of PGAM activity impairs proliferative capacity (Evans *et al.* 2005; Kondoh *et al.* 2005; Hitosugi *et al.* 2012, 2013). Consistently, SIRT2-WT-expressing HCT116 cells exhibited lower proliferation ability when compared to controls

(Fig. 4E). Together, these observations suggest that SIRT2 negatively regulates PGAM activity via its deacetylation and attenuates cell proliferation.

Exploring the lysine acetyltransferases responsible for PGAM

To identify the lysine acetyltransferases (KATs) responsible for PGAM, HCT116 cells were separately transfected with three acetyltransferases, namely PCAF, CBP, and p300, that are known to target nonhistone proteins for acetylation (Roth *et al.* 2001). In PCAF-expressing cells, PGAM1 acetylation was significantly increased in comparison to that in CBP- or p300-expressing, and control cells (Fig. 5A). We further examined the interaction between PGAM and PCAF. To this end, we co-transfected either 3xHA-tagged PGAM1, 3xHA-tagged PGAM2, or empty vector along with FLAG-tagged PCAF, into HCT116 cells. The transfected cells were subjected to immunoprecipitation. As shown in Fig. 5B, C, both PGAM1 and PGAM2 interacted with PCAF. To validate endogenous PCAF-dependent acetylation of PGAM, we used an shRNA-based knockdown approach. HCT116 cells were infected with retroviruses encoding shRNA against PCAF with two different targeting sites (#1 and #2) and selected by puromycin treatment. The knockdown efficiencies for endogenous PCAF were confirmed by real-time PCR analysis (Fig. 5E). However, PGAM acetylation remained unchanged in PCAF knockdown cells (Fig. 5D), suggesting that although endogenous PCAF is not responsible for PGAM acetylation in HCT116 cells, its over-expression can induce PGAM acetylation. To identify the sites of PGAM that are acetylated by PCAF, PCAF was co-transfected with either PGAM1 WT, K100/106/113/138R (referred to as Cent 4KR), or K251/253/254R (referred to as C-ter 3KR) mutants, and their acetylation levels were examined. As shown in Fig. 5F, although acetylation levels of both PGAM1 WT and Cent 4KR were increased by PCAF expression, that of PGAM1 C-ter 3KR was not. Collectively, these data suggest that PCAF is one of the acetyltransferases for PGAM, and its acetylation sites are at the C-terminal (K251/253/254), but not the central, lysines. We examined the endogenous PCAF expression levels of HCT116 cells, comparing them with that of HEK293 cells, in which the C-terminus of PGAM is shown to be highly acetylated (Hallows *et al.* 2012). Interestingly, PCAF expression levels were patently lower in HCT116 cells, compared with HEK293 cells (Fig. S2, in Supporting Information), which suggests that the low acetylation levels in the C-terminus of PGAM in HCT116 cells may be due to low expression levels of endogenous PCAF.

Lysine-to-arginine substitutions at the central region of PGAM impair cell proliferation in HCT116 cells

To examine the effect of the acetylated central lysines on PGAM, we measured enzyme activity using PGAM mutants. The lysines (K100/106/113/138) were mutated to arginines or glutamines, referred to as Central 4KR or 4KQ, respectively. As lysine 138 was not reported to be acetylated by proteomics analysis, we also created mutants without K138R or K138Q substitutions, referred to as Central 3KR or 3KQ, respectively. All four mutants exhibited reduced PGAM activity, to approximately 5% of WT PGAM (Fig. 6A; T. Tsusaka and H. Kondoh, unpublished data). Next, to assess the effect on cell proliferation, PGAM1 WT or Central 3KR mutant were stably expressed in HCT116 cells, and a proliferation assay was carried out after knockdown of endogenous PGAM in these stable cell lines (Fig. 6B, left panel). Central 3KR-expressing HCT116 cells exhibited lower proliferation ability when compared to WT PGAM1-expressing cells (Fig. 6B, right panel). Thus, the substitution of the three lysines (100, 106, and 113) in PGAM abolishes its activity, which may lead to the observed impairment of HCT116 cell proliferation.

Discussion

Here, we report that PGAM interacts with and is deacetylated by SIRT2. Abrogation of PGAM acetylation by ectopic expression of SIRT2 or mutations at the acetylatable lysines of PGAM's central region clearly down-regulates its enzymatic activity. Thus, PGAM is partly regulated by acetylation and deacetylation, which is consistent with evidence showing that PGAM activity is under heavy post-translational regulation (Shalom-Barak & Knaus 2002; Hitosugi *et al.* 2013; Mikawa *et al.* 2014).

In Figure 1, we examined the acetylation levels, protein levels, and enzymatic activities of PGAM, and we noticed, in HCT116 cells, the interesting correlation between highest acetylation and highest enzymatic activity. This led us to the hypothesis that acetylation increases the enzymatic activity of PGAM. Consistently, the decreased acetylation in SIRT2

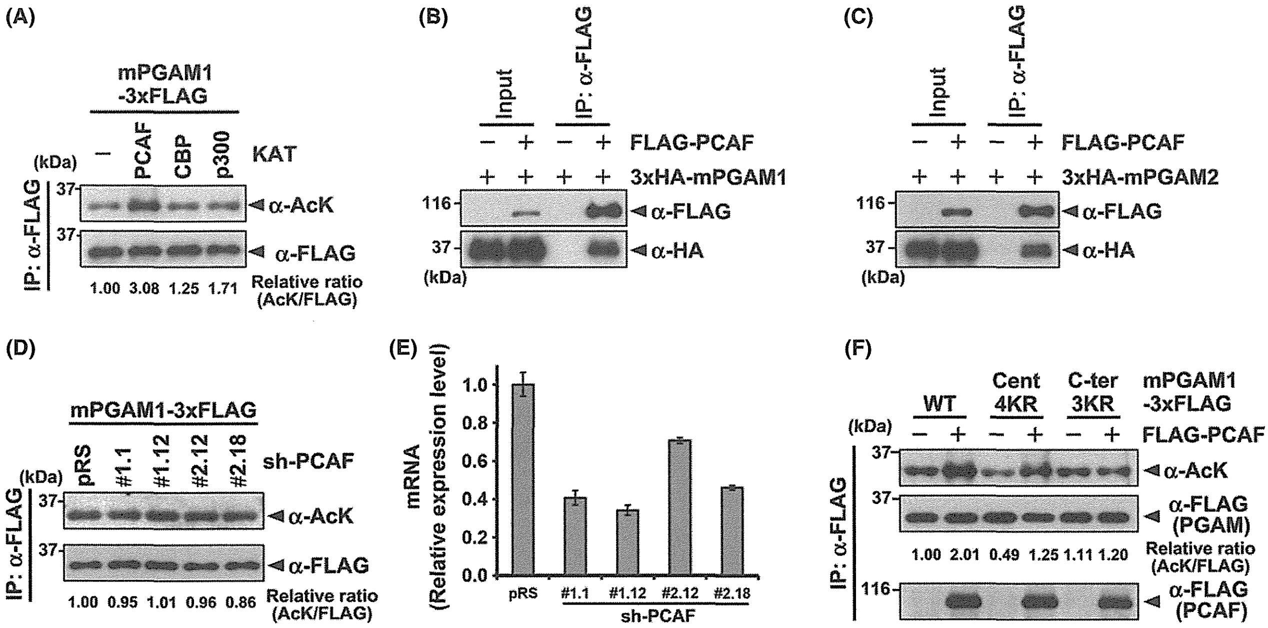

Figure 5 PCAF is one of the acetyltransferases of PGAM and acetylates its carboxyl-terminus, but not its central regions. (A) HCT116 cells were co-transfected with 3xFLAG-tagged PGAM1 vector and either empty control, PCAF-, mCBP-, or p300-expression vector. The PGAM acetylation levels were assessed using antipan acetylated lysine (AcK) or FLAG antibodies as probes after immunoprecipitation (IP) with FLAG M2 affinity gel. (B, C) FLAG-tagged PCAF was co-transfected with 3xHA-tagged PGAM1 (B), PGAM2 (C) or empty vector in HCT116 cells. The cells extracts were subjected to immunoprecipitation (IP) with FLAG M2 affinity gel followed by Western blot analysis with the indicated antibodies. (D, E) HCT116 cells were stably transfected with shRNA against PCAF (#1 and #2, and two clones for each shRNA; #1.1, #1.12 and #2.12, #2.18 are same sequences) or empty vector control. 3xFLAG-tagged wild-type PGAM1 was transiently expressed in the stably transfected cells. The PGAM acetylation levels were assessed using antipan acetylated lysine (AcK) or FLAG antibodies as probes after immunoprecipitation (IP) with FLAG M2 affinity gel (D). Knockdown efficiencies of PCAF were confirmed by real-time PCR analysis (E). Error bars represent SEM ($n = 3$). (F) Central region- (where lysines 100/106/113/138 were mutated to arginines; Cent 4KR) and carboxyl-terminal (where lysines 251/253/254 were mutated to arginines; C-ter 3KR) lysine residues of PGAM1 were mutated, and these mutants and wild-type mPGAM1 were transiently expressed in HCT116 cells. The acetylation of mPGAMs was assessed using antipan acetylated lysine (AcK) or FLAG antibodies as probes after immunoprecipitation (IP) with FLAG M2 affinity gel.

WT-expressing cells or Central 3KR/3KQ PGAM mutants showed decreased enzymatic activity (Figs 4 and 6, respectively). However, in SW620 cells, although the acetylation levels of PGAM were not the lowest, the enzymatic activities were the lowest (Fig. 1). This might be due to other post-translational modifications, such as phosphorylation. Therefore, combined studies of acetylation and other modifications would be required in the future.

Through a comprehensive analysis (Fig. 2), we identified lysines 100, 106, 113 (and possibly also 138) in the central region of PGAM as the acetylated residues in colon cancer HCT116 cells, where enhanced enzymatic activity of highly acetylated PGAM is observed. Consistently, acetylation in the central region of PGAM is also observed in other cell types (e.g. K100 in liver and acute myeloid leukemia cells, K106 in HeLa cells, K113 in acute myeloid leukemia cells), as shown by global proteomic analyses (Kim *et al.* 2006; Choudhary *et al.* 2009; Hebert *et al.* 2013). However, according to Hallows *et al.* (2012), in HEK293 cells, lysines 251, 253, and 254 in the C-terminal region of PGAM are the main acetylated residues, implicating that acetylation sites of PGAM might be regulated in a cell type-dependent manner. Moreover, previous studies and our present work implicate that deacetylases for PGAM are also diverse in different cell lines; SIRT2 for the central region in HCT116 cells and SIRT1 for the C-terminus in HEK293 cells. Interestingly, both SIRT1 and SIRT2 down-regulate PGAM activity by deacetylation. It is not clear why differential deacetylation of PGAM by different Sirtuins regulates its activity in a similar fashion. It is possible that several Sirtuins might have

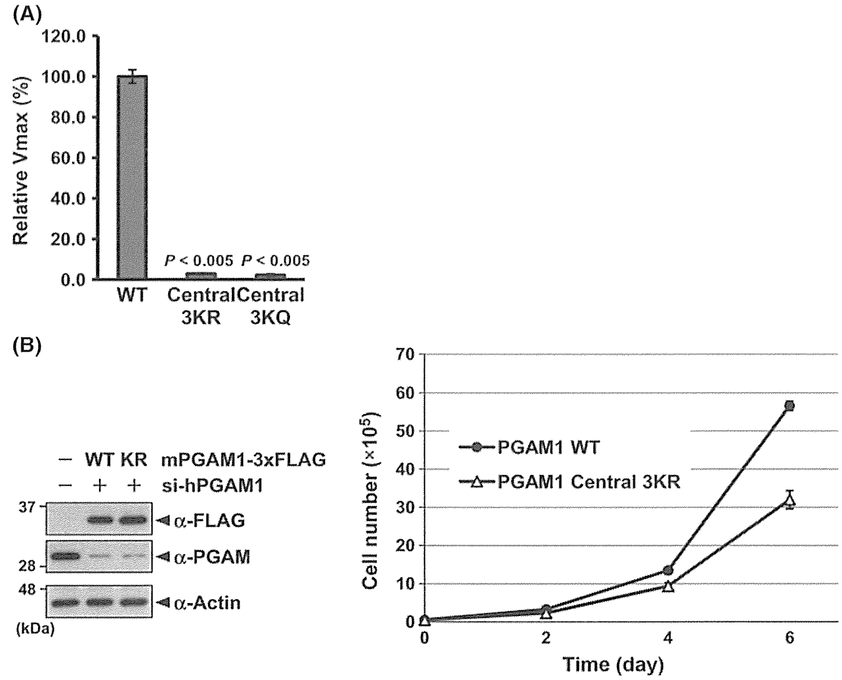

Figure 6 (A) FLAG-tagged wild-type, Central 3KR (K100/106/113R) or Central 3KQ (K100/106/113Q) PGAM1 were transfected into HCT116 cells, and these PGAM proteins were immunoprecipitated by FLAG M2 affinity gel. PGAM activity was measured using immuno-purified PGAM. Error bars represent SEM (n = 3). Statistical analysis was carried out using a *t-test*. (B) HCT116 cells were stably transfected with wild-type or Central 3KR mouse PGAM1, and these cells were subsequently transfected with siRNA against endogenous human PGAM1. At 24 h post-transfection, the cells were re-plated for the proliferation assay (right panel) or Western blot analysis (left panel). Error bars represent SD.

common substrates among their multiple targets, whereas their functional interaction could be cellular-context and cellular-condition dependent. Thus, both SIRT1 and SIRT2 target PGAM, but the contexts in which they are needed might be quite different. Further studies would be required to show the link or difference between deacetylation of PGAM by SIRT1 and that by SIRT2.

To verify the physiological significance of acetylation on the different lysine residues, the identification of the acetyltransferase responsible for acetylation of PGAM would also be crucial. Our attempt using an siRNA library failed to identify the specific acetyltransferase for the central region of PGAM (T. Tsusaka and H. Kondoh, unpublished data), which might require accessory proteins or novel regulational systems. It was observed that acetyltransferase PCAF might play a role in acetylation of PGAM in its C-terminus. Unexpectedly, ectopic expression of PCAF did not affect PGAM enzymatic activity in HCT116 in our experimental conditions (T. Tsusaka and H. Kondoh, unpublished data), although it augments its acetylation in C-terminus even when the central region is acetylated. It is possible that the acetylation in the central regions could have redundant effects with that in the C-terminus.

Previous studies suggest that SIRT2 is a tumor suppressor, as supported by the following results: (i) SIRT2 is down-regulated in gliomas, and its ectopic expression in glioma cell lines leads to significant reduction of colony formation (Hiratsuka *et al.* 2003); (ii) SIRT2 knockout mice show gender-specific tumorigenic phenotypes, and its reduced expression levels are observed in human breast cancers and hepatocarcinoma samples (Kim *et al.* 2011); (iii) Vaquero's group made another line of SIRT2 knockout mice, which are more prone to tumorigenesis in a DMBA/TPA-induced skin tumorigenesis assay, when compared to wild-type mice (Serrano *et al.* 2013). However, the precise role of SIRT2 on enhanced glycolysis in tumors (Warburg effect) is controversial. SIRT2 positively regulates Lactate dehydrogenase A (LDH-A), a glycolysis-related enzyme, and promotes pancreatic cancer proliferation (Zhao *et al.* 2013); whereas SIRT2 negatively regulates HIF-1, in HeLa cells (Seo *et al.* 2014). Our data show that SIRT2 negatively regulates PGAM in colon cancer HCT116 cells, supporting the notion that SIRT2 might function as a tumor suppressor by attenuating the Warburg effect. Collectively, PGAM acetylation and its regulation by SIRT2 could be possible therapeutic targets in the future, as inhibition of PGAM activity impairs cancerous proliferation (Evans *et al.* 2005; Hitosugi *et al.* 2012).

Experimental procedures

Plasmids

p3xFLAG-CMV14 (Sigma-Aldrich) vectors encoding mouse PGAM1 or PGAM2 have been described previously (Mikawa *et al.* 2014). Lysine mutants of PGAM1 and PGAM2 were generated by PCR-based site-directed mutagenesis. The human Sirtuin (SIRT1-7) expression plasmids were a kind gift from Dr. E. Michishita-Kioi. The SIRT1 and SIRT2 cDNA with V5-tag sequence were subcloned into pBabe.puro retroviral vector. The catalytically inactive SIRT2 mutant (H187Y) was generated by PCR-based site-directed mutagenesis. The lysine acetyltransferase (KAT) expression vectors were obtained from Addgene. To generate shRNAs against human PCAF, the relevant DNA oligonucleotides were annealed and ligated into the HindIII and BglII sites of pRetro.Super (pRS) vector (Oligoengine; Brummelkamp *et al.* 2002). To make 3xHA-tagged PGAM1 and PGAM2 expression vectors, the mouse PGAM1 and PGAM2 cDNAs were subcloned into pcDNA-3.1 (-)-3xHA vector (Mikawa *et al.* 2014). The 3xFLAG-tagged mouse PGAM1 wild-type or K100/106/113R mutant DNA fragments were subcloned into pHygro Marx IV retrovirus vector.

Details are described in Table S1 and S2, in Supporting Information.

Cell culture, DNA/RNA transfection, and retrovirus infection

Human cell lines (HCT116, DLD-1, SW480, SW620, SW48, RKO, and PLAT-A) were cultured in Dulbecco's modified Eagle's medium (Nacalai) supplemented with 10% fetal bovine serum. DNA transfection was carried out using Polyethylenimine Max (Polyscience, Inc.; for HCT116, DLD-1, SW480, SW620, RKO, and PLAT-A) or Lipofectamine 2000 (Invitrogen; for SW48), according to the manufacturer's instructions. PLAT-A packaging cell lines were used for retrovirus production. Infected cells were subsequently subjected to drug selection with the addition of hygromycin (250 μg/mL) or puromycin (2.2 μg/mL), as required. After drug selection, the cells were subjected to further manipulations or analyses. RNA transfection was carried out using Lipofectamine RNAi Max (Invitrogen), according to the manufacturer's instructions.

Western blot and real-time PCR analysis

For Western blot analysis, cell lysates were prepared as described previously (Mikawa *et al.* 2014). Briefly, the cells were harvested after trypsinization, washed twice with ice-cold PBS, and lysed with lysis buffer (50 mM Tris-HCl at pH 7.5, 200 mM NaCl, 1 mM EDTA, 10% glycerol, 0.5% Triton X-100, 50 mM NaF, 1 mM DTT, 1 mM phenylmethanesulfonyl fluoride, 5 mM nicotinamide, and 5 M tricostatin A; Sigma-Aldrich, and 1× protease inhibitor cocktail; Nacalai). The cell lysates were subjected to protein assay (Bio-Rad). Equivalent amounts of protein were resolved by SDS-PAGE. The antibodies used in this study are described in the Antibodies section. Densitometric analysis was carried out using ImageJ software (version 1.45s, downloaded from http://imagej.nih.gov/ij/).

For real-time PCR analysis, total RNA was isolated using Trizol (Invitrogen). cDNAs were generated using ReverTra Ace qPCR RT Master Mix (Toyobo). real-time PCR analysis was carried out using Thunderbird SYBR qPCR Mix (Toyobo). Each mRNA levels were normalized by Rpl13a mRNA. The primers used in these analyses are described in Table S2, in Supporting Information.

Immunoprecipitation

For immunoprecipitation, cell lysates were lysed with lysis buffer (50 mM Tris-HCl at pH 7.5, 200 mM NaCl, 1 mM EDTA, 10% glycerol, 0.5% Triton X-100, 50 mM NaF, 1 mM DTT, 1 mM phenylmethanesulfonyl fluoride, 5 mM nicotinamide and 5 M tricostatin A; Sigma-Aldrich, and 1× protease inhibitor cocktail; Nacalai). After centrifugation at 14 000 ***g*** for 10 min, the supernatants were incubated with anti-FLAG affinity gel (Sigma-Aldrich) for 4 h or overnight at 4 °C. The resin was then washed four times with wash buffer (50 mM Tri-HCl at pH 7.5, 200 mM NaCl, 1 mM EDTA, 10% glycerol, 0.5% Triton X-100, 50 mM NaF, 1 mM DTT, 1 mM phenylmethanesulfonyl fluoride) and eluted using 2× Laemmli sample buffer. The eluate was resolved by SDS-PAGE, and gel staining was carried out using CBB Stain One (Nacalai). Equivalent amounts of precipitates were subjected to Western blot analysis.

Antibodies

Antibodies used in this study were as follows: anti-PGAM raised against full-length recombinant mouse PGAM2 protein (Mikawa *et al.* 2014); anti-Actin (AC-40) and anti-FLAG (M2, F3165) from Sigma-Aldrich; anti-Acetylated lysine (AcK, #9441) and anti-PCAF (C14G9, #3378) from CST; anti-V5 (46-0705) from Life Technologies; anti-HA (sc-840) and